Earth-Science Reviews 201 (2020) 103082

Contents lists available at ScienceDirect

Earth-Science Reviews

journal homepage: www.elsevier.com/locate/earscirev

How faithfully do the geochronological and geochemical signatures of detrital zircon, titanite, rutile and monazite record magmatic and metamorphic events? A case study from the Himalaya and Tibet

Ronghua Guo[a], Xiumian Hu[a,*], Eduardo Garzanti[b], Wen Lai[a], Bing Yan[c], Chris Mark[d,1]

[a] School of Earth Sciences and Engineering, Nanjing University, Nanjing 210029, China
[b] Department of Earth and Environmental Sciences, University of Milano-Bicocca, Milano 20126, Italy
[c] College of Oceanography, Hohai University, Nanjing 210098, China
[d] Department of Geology, Trinity College Dublin, Dublin, Ireland

ARTICLE INFO

Keywords:
Provenance analysis
Heavy minerals
Detrital geochronology
Geochemical tracers
Tibet and Himalaya
Lhasa, Nianchu, Pumchu and Yarlung Tsangpo river

ABSTRACT

Detrital geochronology, generally focused on zircon only, is widely used not only to obtain qualitative information on source areas but also in quantitative provenance analysis aimed at calculating sediment yields and erosion rates under the assumption that age spectra broadly reflect the proportions of areal exposures of source rocks. The principal aim of this article is to put this assumption to test. The Tibetan Plateau and Himalayan belt, in which the age of magmatic and metamorphic events has been accurately determined through decades of geological and geochronological studies, represent an excellent natural laboratory for provenance analysis. In this study, we focus on sand carried by three major Tibetan rivers - including the largest tributaries of the Yarlung Tsangpo draining either the Lhasa block or the Himalaya exclusively - and couple classical petrographic and heavy-mineral analyses with geochronological and geochemical fingerprinting of detrital zircon, monazite, titanite, and rutile as witnesses of episodes of crustal growth in their catchment. Zircon, rutile, monazite, and titanite provide different responses to magmatic and metamorphic events and are highly to moderately durable minerals that can be preserved in ancient sandstones, thus representing precious tracers in provenance analysis. Our results show that largely euhedral zircon and titanite grains in Lhasa River sand reflect the multiple magmatic events that affected the Lhasa block through the Mesozoic and Cenozoic, and together with detrital monazite and rutile highlight post-collisional metamorphic events in the Nyainqentanglha Range. Mostly rounded detrital minerals generated in the Nianchu and Pumchu catchments are instead largely recycled from Tethys Himalayan sedimentary rocks, but young ages of monazite and titanite grains reflect the widespread Miocene thermal event associated with leucogranite intrusions both at the top of the Greater Himalayan metamorphic unit and in Northern Himalayan gneiss domes. The geochemical signature of most rutile grains in all studied samples indicates ultimate provenance from metapelites. Most important, the age spectra of different datable detrital minerals reflect poorly and in very different proportions the areal exposure of source-rock lithologies (and in the Lhasa River catchment also the areal exposure of granitoids of different age). We conclude that, although detrital geochronology does provide essential information in qualitative provenance reconstructions, the age distributions of single minerals cannot be reliably converted in terms of proportional sediment yield, and thus cannot be used to calculate sediment budgets or trace erosion rates unless fertility bias is accurately quantified and taken into due account.

1. Introduction

Provenance analysis scrutinizes the stratigraphic archive to restore information forever lost by erosion of bedrocks and provides a way to establish a link between sedimentary deposits and orogenic belts. We can thus make inferences about the location of source areas and their lithological and time structures, with the final goal of reconstructing reliable paleogeodynamic, paleogeographic, and paleoclimatic scenarios (Dickinson, 1985, 1988; Potter, 1994; Garzanti et al., 2007, 2018). During the last decades, high-resolution geochemical

* Corresponding author.
E-mail address: huxm@nju.edu.cn (X. Hu).
[1] Now at: School of Earth Sciences, University College Dublin, Dublin D04 V1W8, Ireland.

https://doi.org/10.1016/j.earscirev.2020.103082
Received 21 March 2019; Received in revised form 10 December 2019; Accepted 7 January 2020
Available online 10 January 2020
0012-8252/

fingerprinting and isotopic dating methods have been widely applied to provenance analysis, with a strong focus on detrital zircon (Gehrels et al., 1995; Fedo et al., 2003; Andersen, 2005; Dickinson and Gehrels, 2009; Cawood et al., 2012; He et al., 2014). Zircon is rich in radioactive Th and U but lacks common Pb, has strong ability to resist subsequent lower-temperature events, and has thus become the most popular target of geochronological dating in sediments and sedimentary rocks (Belousova et al., 2002; Rubatto, 2002; Grimes et al., 2007; Carrapa, 2010). On the other hand, the zircon content in different rock types varies over orders of magnitude, and such a fertility bias thus distorts provenance signals, enhancing those emitted from zircon-rich rocks while concealing those from zircon-poor sources (Moecher and Samson, 2006; Dickinson, 2008; Malusà et al., 2016; Spencer et al., 2018). Because zircon is one of the most resistant minerals to chemical attack during weathering and diagenesis (Carroll, 1953; Morton and Hallsworth, 2007), and can thus survive multiple sedimentary cycles, it is difficult and frequently impossible to establish whether the information it carries relates to igneous or metamorphic rocks exposed while the sediment was generated or during an undefined older sedimentary cycle (Hawkesworth et al., 2009; Garzanti et al., 2013). Other minerals, however, can be used and new approaches beneficially experimented in provenance research (e.g., Morton, 1991; Suzuki and Adachi, 1991; Mange and Morton, 2007; Wang and Hu, 2008; Hietpas et al., 2010; Thomsen et al., 2015; Liu et al., 2017; O'Sullivan et al., 2017).

The progress of technology and the development of EMPA, LA-ICP-MS and SIMS techniques has given a great impulse to provenance analysis, allowing collection of large numerical datasets and thus fostering progress towards quantitative approaches. Age distributions of datable detrital minerals in modern sand reflect diverse events of crustal growth in distinct geological domains within a river catchment and thus potentially allow us not only to pinpoint source areas but even to tentatively reconstruct sediment budgets and trace erosion rates (Molinaroli and Basu, 1993; Weltje and von Eynatten, 2004; Weltje, 2012; Vezzoli et al., 2016a). Such calculations, however, require that the generation potential of the target mineral (fertility) is the same for all rocks exposed in the basin, a precondition that is seldom respected (Malusà et al., 2016, 2017).

The Tibetan Plateau, poetically called “the roof of the world” or “the Asian water tower”, is the source of many large rivers including the Yarlung Tsangpo-Brahmaputra and Indus rivers. Multiple magmatic and metamorphic events that affected Tibet and the Himalaya have long been studied in detail, providing a solid reference for comparison with data obtained from detrital minerals in modern sediments. To this goal, we focused on major Tibetan rivers draining either the Lhasa block (Lhasa River) or the Himalaya exclusively (Nianchu and Pumchu; chu = river in Tibetan language) (Fig. 1).

The Lhasa River and the Nianchu are the largest northern and southern tributaries of the Yarlung Tsangpo, representing the headwaters of the Brahmaputra River in Tibet. In order to obtain a statistical representation of source rocks and erosional processes active in each catchment, we collected bedload sand samples in the final tract of each river, and carried out geochronological and geochemical analyses of detrital zircon, monazite, titanite, and rutile contained in modern sands as witnesses of magmatic and metamorphic events of crustal growth in the source area. We compared homologous data from modern daughter sediments and ancient parent rocks to check how faithfully the latter are represented in the former, and whether and in which circumstances the size of age populations can be considered as at least roughly proportional to the areal exposures of source rocks of corresponding ages (Saylor et al., 2013). The purpose of this article is not only to explore new avenues for provenance research by the use of geochronological and geochemical fingerprints of multiple detrital minerals, but also to re-evaluate the relationship between detrital age distributions and areal exposures of source rocks, which represents an essential step to correct for fertility bias and thus achieve accurate assessments of sediment yields and erosion rates.

2. Geological framework

Rocks exposed in southern Tibet along the Yarlung-Tsangpo Suture Zone record the earliest phases of Himalayan orogenesis: the timing of this event is well constrained at ~59 ± 1 Ma (Garzanti et al., 1987; DeCelles et al., 2014; Wu et al., 2014; Hu et al., 2015a, 2016), but the tectonic identity of the colliding blocks during this intial phase remains controversial (Kapp and DeCelles, 2019). The suture zone marks the boundary between Greater Himalayan metamorphic and Tethys Himalayan sedimentary rocks to the south, representing the remnants of the Indian passive continental margin (Gansser, 1964; Ratschbacher et al., 1994; Sciunnach and Garzanti, 2012; Carosi et al., 2018), and the Lhasa block to the north, representing the formerly active continental margin of Asia (Chung et al., 2005; Zhu et al., 2011) (Fig. 1).

2.1. Tethys and Greater Himalaya

The sedimentary succession of the Tethys Himalayan zone includes Paleozoic to Eocene carbonate and siliciclastic rocks (Sciunnach and Garzanti, 2012) that contain zircon grains yielding U—Pb ages clustering around 500 Ma and 1100 Ma (DeCelles et al., 2000, 2004; Gehrels et al., 2011). Pre-collisional magmatic rocks include Lower Permian basalts (Garzanti et al., 1999; Yin et al., 2006) and Lower Cretaceous volcanic and volcaniclastic rocks (Jadoul et al., 1998; Zhu et al., 2005, 2007, 2009), the latter yielding detrital zircons dated between 110 Ma and 150 Ma (Hu et al., 2010, 2015b).

An alignment of gneiss domes define the Northern Himalayan antiform, grown in the hanging-wall of the north-dipping Gyirong–Kangmar thrust and separating the northern and the southern Tethys Himalayan domains (Ratschbacher et al., 1994) (Fig. 1). The core of the domes is formed by granitoids and migmatitic orthogneisses of Early Paleozoic age associated with Miocene leucogranitic melts, overlain by Paleozoic and Mesozoic metasedimentary rocks ranging in metamorphic grade from upper amphibolite-facies at the base to very-low-grade at the top (Lee et al., 2000, 2004).

Crystalline rocks of the Greater Himalaya record polyphase magmatic and metamorphic events and yield zircons with U—Pb ages clustering around 500 Ma, 850 Ma, 1.1 Ga, 1.5–1.8 Ga, and 2.5–2.6 Ga (DeCelles et al., 2000, 2004; Gehrels et al., 2011). Miocene leucogranites widely occur at the top of the Greater Himalaya (Harrison et al., 1998; Wu et al., 2015) and Eocene granites are found in Northern Himalayan gneiss domes (Zeng et al., 2011). Multiple metamorphic events in the Greater Himalaya lasted from ~44 to ~4 Ma (Aikman et al., 2008; Kohn, 2014; Goscombe et al., 2018).

2.2. Lhasa block

The Lhasa block includes a northern terrane with Mesozoic strata and a central terrane with low-grade Carboniferous-Permian metasedimentary rocks and Mesozoic volcano-sedimentary sequences intruded by Mesozoic batholiths (Pan et al., 2004; Chung et al., 2005; Chu et al., 2006; Zhu et al., 2011) (Fig. 1). The southern terrane, where granitoid rocks of the Gangdese arc batholith are widespread (Fig. 1), includes uppermost Triassic to Cretaceous sedimentary rocks, Jurassic-Lower Cretaceous volcanic rocks, and Upper Cretaceous to Eocene Linzizong andesites to rhyolitic ignimbrites (Wen et al., 2008; Ji et al., 2009; Zhu et al., 2011, 2013). Multistage magmatic activity in the southern Lhasa terrane was recorded most prominently between 41 and 65 Ma, preceded by episodes at 152–205 Ma and 80–109 Ma (Chung et al., 2005; Zhu et al., 2011, 2019). Post-collisional magmatic activity in the Oligocene-Miocene (10–33 Ma) is documented by small intrusions, veins and lavas of adakitic, potassic, and peraluminous rocks (Turner et al., 1993; Miller et al., 1999; Ding et al., 2003; Zhao et al., 2009; Ji et al., 2009; Liu et al., 2011). Only locally exposed basement rocks of the

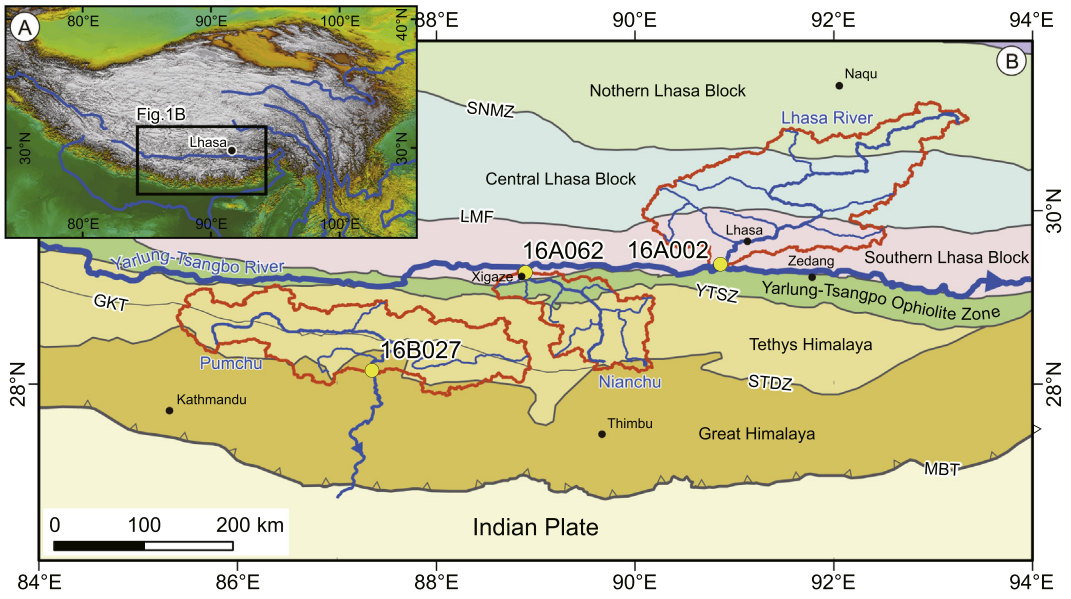

Fig. 1. Simplified geological map of the Himalayan Range and the southern Tibetan Plateau (after Pan et al., 2004). A) Digital topographic map based on SRTM data. B) Catchment areas of the Lhasa River, Nianchu and Pumchu (circled in orange) with location of samples 16A001, 16A062 and 16B027 (yellow dots). MBT: Main Boundary Thrust; STDZ: South Tibet Detachment Zone; GKT: Gyirong-Kangmar Thrust; YTSZ: Yarlung-Ysangpo Suture Zone; LMF: Luobadui Milashan Fault; SNMZ: Shiquanhe NamTso Mélange Zone. (For interpretation of the references to colour in this figure legend, the reader is referred to the web version of this article.)

Lhasa Block recorded multiple metamorphic events since the Late Neoproterozoic and Early Paleozoic, as documented in the northern terrane and in the Nyainqentanglha Range (Xu et al., 1985; Zhang et al., 2014).

3. Lhasa, Nianchu and Pumchu river catchments

The topographic maps of the Lhasa, Nianchu and Pumchu river catchments were obtained by analyzing Shuttle Radar Topography Mission (SRTM) 90 m Digital Elevation Model (DEM) data (Jarvis et al., 2008) in ArcGIS 10.2, and the corresponding geological maps from the Global Mapper (1:1,500,000 geological map after Pan et al. (2004)) using the Cylindrical Equal Area (world) coordinate system. By plotting the two maps together in ArcGIS we could calculate the areal exposure for each different lithology as well as for plutonic and volcanic rocks of different ages in the Lhasa River catchment.

3.1. Lhasa River

The Lhasa River, the largest left-bank (northern) tributary of the Yarlung Tsangpo, drains the Nyainqentanglha Range, the northern central and southern terranes of the Lhasa Block (Fig. 1). Exposed in the catchment are mainly sedimentary rocks (very-low-grade Carboniferous-Permian metasediments, 58.1%), Mesozoic to Cenozoic Gangdese plutonic (27.1%) and Linzizong volcanic rocks (12.1%), lakes and glaciers (2.0%), and a few metamorphic rocks (0.7%) (Fig. 2). The areal exposure of Jurassic, Cretaceous, Paleogene, and Neogene granitoids is 0.3%, 11.3%, 12.4% and 3.1%, respectively. Metamorphic rocks including gneiss, schist, amphibolite, and marble are exposed in the Nyainqentanglha Range, forming the western divide of the catchment, and document high-temperature deformation events at 13–28 Ma, 30–65 Ma, 90–120 Ma, and 213–225 Ma (Xu et al., 1985; Hu et al., 2003; Kapp et al., 2005; Zhang et al., 2014) (Appendix Table 1-a). Detrital zircons contained in Carboniferous-Permian strata cluster at 100–150 Ma, 500–600 Ma, and 1000–1400 Ma (Leier et al., 2010).

3.2. Nianchu

The Nianchu is the largest right-bank (southern) tributary of the Yarlung Tsangpo, with confluence near the city of Xigaze. Sourced from the northern flank of the Greater Himalaya, the river flows northwards in the Tethys Himalayan zone, cutting across the Kangmar gneiss dome and finally draining ophiolites, ophiolitic mélange, and forearc strata of the Yarlung-Tsangpo suture (Fig. 1). Sedimentary rocks (including Permo-Triassic slate) occupy most of the catchment (90.7%; Fig. 2), the rest being accounted for by ophiolite (5.3%), igneous rocks (2.4%, mainly leucogranite), metamorphic rocks (1.2%), and lakes (0.4%).

Several Greater Himalayan and Northern Himalayan leucogranite bodies yielding Miocene U-Th-Pb monazite ages occur in the Nianchu basin (Fig. 2), including the Wanye La leucogranite (11.9 Ma) (Wu et al., 1998). The Kangmar gneiss dome yielded U—Pb zircon ages between 460 Ma and 1144 Ma (Appendix: Table 1-b). Metamorphic wallrocks of leucogranites, including schist, gneiss and granulite, yielded ages ranging from 17 to 30 Ma for Yadong (Zhang et al., 2015; Li et al., 2015) to 10–36 (Ar/Ar mica) or 20–160 Ma (U-Th-Pb monazite) for Kangmar (Hacker et al., 2011; Wang et al., 2015) (see Appendix: Table 1-c). Permo-Triassic slates yielded zircon ages clustering at 480–570 Ma, 750–1200 Ma, and 2430–2560 Ma (Gehrels et al., 2011).

3.3. Pumchu

The Pumchu originates from the Yebokang Gale Glacier of the 8012 m-high Xixiabangma massif. The river flows northwestward at first, and next eastward across sedimentary rocks of the Tethys Himalaya (Fig. 1), which account for 78.9% of the considered Tibetan part of the catchment. Downstream, the river turns southwestward and next southward to leave Tibet and cut across the entire Himalayan belt in Nepal where it is called Arun and represents one major branch of the Sapt Kosi, in turn a large tributary of the Ganga River in India. Metamorphic rocks, igneous rocks (mainly leucogranite) and glaciers account for 9.5%, 4.8%, and 6.8% of the remaining part of the considered Tibetan catchment (Fig. 2).

Numerous Greater Himalayan and Northern Himalayan leucogranite bodies (Fig. 2) yielding Miocene ages occur in the Pumchu basin (Appendix Table 1-b): Majia (U-Th-Pb zircon, monazite, xenotime; 8–23 Ma) (Lee et al., 2006; King et al., 2011), Lhagui Kangri (U-Th-Pb zircon, monazite; 14–15 Ma) (Schärer et al., 1986; Zhang et al., 2005),

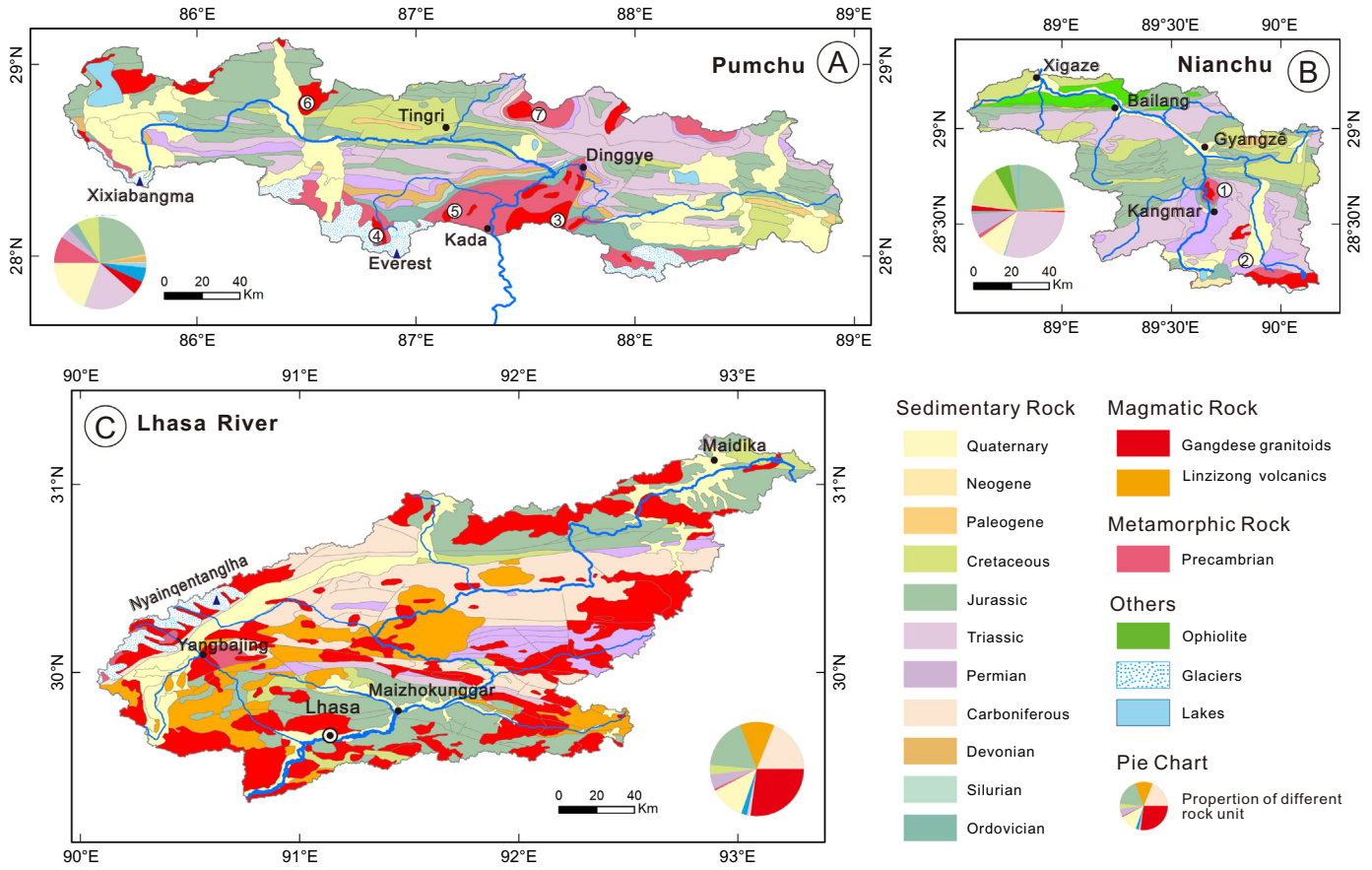

Fig. 2. Geological maps of the Pumchu (A), Nianchu (B) and Lhasa River (C) catchments (after Pan et al., 2004). Pie charts indicate the relative proportions of exposure areas for different lithological units. Leucogranite-bearing Himalayan domes (white circles): 1, Kangmar; 2, Wagye La; 3, Dinggye; 4, Rongbuk; 5, Everest-Makalu; 6, Lhagoi Kangri; 7, Majia.

Everest-Makala (U-Th-Pb zircon, monazite; 14–24 Ma) (Streule et al., 2010), Dingye (U-Th-Pb zircon, monazite; 12–20 Ma) (Leloup et al., 2010) and Rongbu (U-Th-Pb monazite: 15–22 Ma) (Cottle et al., 2015). Metamorphic wallrocks of leucogranites, including schist, gneiss, and granulite, yielded Oligo-Miocene and thus only slightly older U—Pb zircon, U-Th-Pb monazite, and Ar/Ar mica ages (Appendix Table 1-c): Majia (U-Th-Pb monazite; 20–29 Ma) (Lee et al., 2006), Everest-Makala (U-Th-Pb zircon, monazite; 12–30 Ma) (Cottle et al., 2011), and Dingye (U-Th-Pb zircon, monazite; 12–30 Ma; Ar/Ar mica; 14–15 Ma) (Leloup et al., 2010).

4. Methods

Three big (5 kg) sand samples were collected on active sand bars in the final tract of the Lhasa (Kyi) River (sample 16A002; GPS coordinates: N29.374250, E90.859500) and of the Nianchu (upstream of the confluence with the Yarlung Tsangpo: sample 16A062; GPS coordinates: N29.284611, E88.894694), and in the Pumchu upstream of the political border with India (sample 16B027; GPS coordinates: N 28.159988, E 87.346076) (Figs. 1, 2). A quartered aliquot of each bulk sample was impregnated with araldite, cut into a standard thin section stained with alizarine red to distinguish dolomite and calcite, and analysed by counting 450 points under the microscope (Gazzi-Dickinson method; Ingersoll et al., 1985). Sand classification was based on the main components quartz (Q), feldspars (F), and lithic fragments (L), considered if > 10% QFL (e.g., a sand is named litho-feldspatho-quartzose if Q > F > L > 10% QFL; Garzanti, 2016, 2019). Heavy-mineral analyses were carried out on a quartered aliquot of the 32–500 μm class obtained by dry-sieving. Heavy minerals were separated by centrifuging in sodium polytungstate (density ~2.90 g/cm^3) and recovered by partial freezing with liquid nitrogen. On grain mounts, 200–250 transparent heavy-mineral grains were point-counted at a suitable regular spacing under the petrographic microscope to obtain real volume percentages (Galehouse, 1974). Significant detrital components are listed in order of abundance (high to low) throughout the text.

Detrital zircon, monazite, titanite, and rutile were separated by standard heavy-liquid and magnetic methods at Langfang Geological Service Co., LTD (www.lfcxdz.com). Mineral grains were attached to double-sided tape using a binocular microscope. The oxygen resin and the curing agent are mixed with a ratio of 15:2, and then cured at room temperature. The grain surface was polished first with 3000 mesh, 5000 mesh, and 7000 mesh sandpaper; next, 8000 mesh and 10,000 mesh diamond polishing cream was used to expose internal surfaces. For each mineral, 120–130 grains were used for geochemical and geochronological analyses. The relevant age ratios and isotopic ratios for zircon, titanite, and monazite were calculated using GLITTER 4.4; rutile U—Pb data were reduced using the VisualAge. UComPbine data reduction scheme (DRS) for Iolite (Chew et al., 2014; Paton et al., 2010). Age calculations and probability density mapping were performed using Density Plot 8.2 (Vermeesch, 2012).

4.1. Detrital zircon geochronology

U-Th-Pb dating of detrital zircons was carried out by laser ablation-inductively coupled plasma-mass spectrometry (LA-ICP-MS) at the State Key Laboratory for Mineral Deposits Research, Nanjing University with an Agilent 7500a quadrupole rod spectrometer and a New Wave's UP-

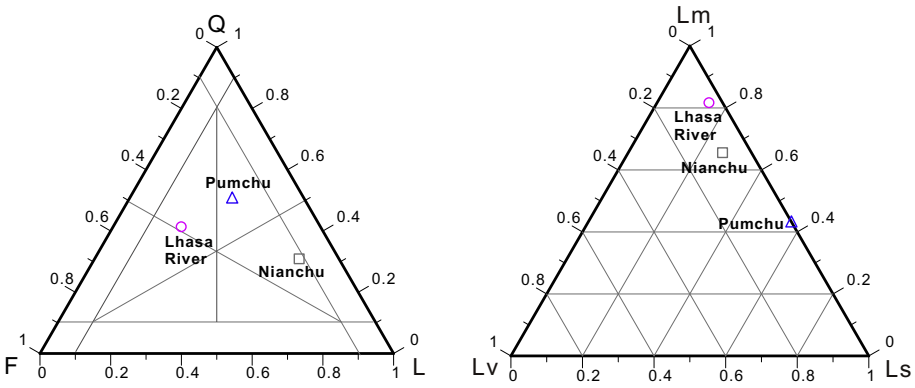

Fig. 3. Petrographic modes of Lhasa, Nianchu an Pumchu river sands. Classification scheme after Garzanti, 2016, 2019. Average modes: Lhasa River, Q:F:L = 42:39:19; Nianchu Q: F: L = 31:11:58; Pumchu Q: F: L = 50:19:3. Q, Quartz; F, Feldspar; L, Lithic fragments (Lv, volcanic; Lm, metamorphic; Ls, sedimentary).

213 solid-state laser ablation system (laser spot diameter 35 μm). GJ-1 (608.5 ± 1.5 Ma) and Mud Tank (732 ± 5 Ma) analytical standards were used (Black and Gulson, 1978). Isotope ratios and age errors for single-point analysis are expressed as 1σ (test principles, data processing, and Pb correction methods as in Jackson et al., 2004). Common Pb correction was made using Com-Pbcorr3-16 fl (Andersen, 2002). We used $^{206}Pb/^{238}U$ and $^{207}Pb/^{206}Pb$ ages for zircons younger and older than 1000 Ma, respectively. Ages were discarded if discordance was > 20% for grains younger than 200 Ma or > 10% for older grains.

4.2. Detrital monazite and titanite geochronology

Monazite and titanite were dated using multi-collector (MC) ICP-MS at the Institute of Geology and Geophysics of the Chinese Academy of Sciences, Beijing with an Agilent 7500a quadrupole spectrometer. U-Th-Pb dating of detrital monazite was performed according to Liu et al. (2012), using JEFF (364 Ma) and M1 (525 Ma) as internal standards (Peterman, 2005) and M4 (519 Ma) as external standard (Liu et al., 2012). The excitation environment is 3 Hz, 130 counts, the laser spot diameter is 40 μm, and standard samples are 25 μm. No common Pb correction was made. Because monazite is Th-rich, leading to an excess of ^{206}Pb and thus to an overestimation of the U−Pb age, the $^{208}Pb/^{232}Th$ age was used instead, with analytical error expressed as 1σ. Trace elements were tested with NIST610 as external standard and Ce as normalized element by using software GLITTER 4.0 (Griffin et al., 2008), following Buick et al. (2010).

U-Th-Pb dating of titanite was performed according to Sun et al. (2012), using BLR (1048 ± 0.7 Ma) as internal standard (Aleinikoff et al., 2002) and OLT (1014.8 ± 2 Ma) as external standard (Kennedy and Nasdala, 2002). The excitation environment is 8 Hz, 350 counts, and the laser spot diameter is 40 μm. We made the ^{207}Pb correction and used the $^{206}Pb/^{238}U$ age with analytical error expressed as 1σ. Trace elements were tested with NIST 610 glass as external standard and Ca as normalized element by using software GLITTER 4.0 (Griffin et al., 2008).

4.3. Detrital rutile geochronology

U-Th-Pb dating of detrital rutile was carried out at Trinity College (Dublin, Ireland) using a Photon Machines Analyte Exite 193 nm ArF excimer laser-ablation system coupled to an Agilent 7700 quadrupole ICP-MS. Spot sizes were 40 or 50 μm (in separate sessions) as grain size dictated, with a fluence of 2.5 Jcm^{-2} and a repetition rate of 20 Hz; masses for U−Pb geochronology and trace-element analysis (^{52}Cr and ^{93}Nb, plus ^{49}Ti as an internal stochiometric standard) were monitored during the same duty cycle. The primary standard was R10 rutile; R19, RZ3, Sugluk, and PCA rutiles (Luvizotto et al., 2009; Shi et al., 2012; Bracciali et al., 2013) were employed as secondary standards and treated as unknowns during data reduction and age calculation. The secondary standards respectively yielded weighted mean ^{207}Pb-corrected ages of 495 ± 5 Ma, 1796 ± 20 Ma, 1724 ± 17 Ma, and 1903 ± 17 Ma, all of which are indistinguishable from accepted ages at the 2σ except PCA, which is ca. 0.7% too old. Data reduction used the VisualAge_UComPbine data reduction scheme (DRS) for Iolite (Chew et al., 2014; Paton et al., 2010). As rutile is frequently discordant in the U−Pb isotopic system a ^{207}Pb-based correction was employed to correct for the effects of common-Pb (Pb_c, Pb incorporated during crystal growth as opposed to radiogenic Pb generated by in-situ radionuclide decay, Pb*), as described by Chew et al. (2011). As many grains were discordant, a classical discordance filter could not be applied (e.g., Gehrels et al., 2011); however, high Pb_c/Pb^* values for some grains were reflected in undesirably large age uncertainties. Therefore, the following age uncertainty filters were employed: < 25% for ages > 100 Ma; 25–50% for ages between 10 and 100 Ma; and < 100% for ages < 10 Ma. All ages are reported at the 2σ-level.

Rutile trace element abundances were calculated using the Trace_Elements DRS in Iolite, implementing the internal elemental standard approach of Woodhead et al. (2007). NIST612 was employed as the primary standard, and R10 as the secondary standard which was treated as an unknown during data reduction and yielded Cr and Nb concentrations of 675 ± 29 ppm and 2623 ± 24 ppm, respectively, which are indistinguishable at 2σ-level from the values reported by Luvizotto et al. (2009).

5. Petrography and heavy minerals

Sand transported in the lower course of the Lhasa River draining the Lhasa block and the Gangdese arc is litho-feldspatho-quartzose with plagioclase > K-feldspar (Fig. 3). Microlitic to felsitic volcanic, shale/slate/phyllite, siltstone/metasiltstone, metadacite, chloritoschist, and rare high-rank metamorphic rock fragments occur. Micas are common (biotite > > muscovite). The moderately rich transparent-heavy-mineral assemblage, dominated by blue-green amphibole, contains epidote and minor garnet, zircon, apatite, and clinopyroxene. For a more detailed description of petrographic and mineralogical signatures of modern sands throughout the Lhasa River catchment the reader may refer to Garzanti et al. (2019).

Sand carried by the Nianchu draining the Tethys Himalaya and Northern Himalaya domains and finally the Yarlung-Tsangpo suture in the lower course is feldspatho-quartzo-lithic with plagioclase > K-feldspar (Fig. 3). Dominant shale to siltstone and slate to metasiltstone grains are associated with carbonate/metacarbonate, metavolcanic, ultramafic (mostly cellular serpentinite), phyllite, and rare higher-rank metamorphic rock fragments. Micas are rare. The moderately poor transparent-heavy-mineral assemblage contains garnet, augitic clinopyroxene, epidote, mostly blue-green amphibole, olivine, tourmaline, zircon, and rarer enstatite, apatite, prehnite, and titanite.

Sand carried by the Pumchu draining the top of the Greater Himalaya and the Tethys Himalaya is feldspatho-litho-quartzose with plagioclase ≈ K-feldspar (Fig. 3). Abundant shale to siltstone and slate

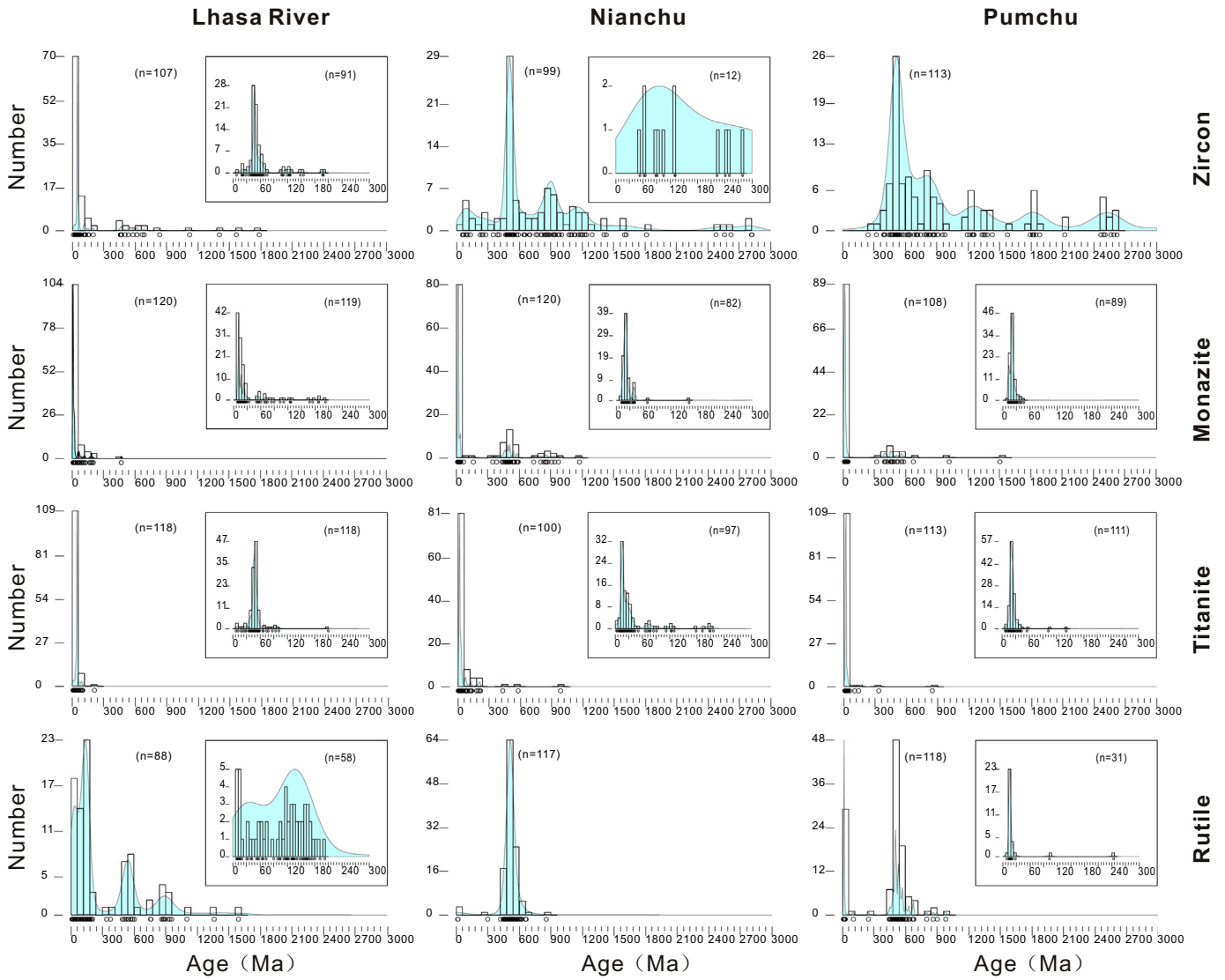

Fig. 4. U−Pb age spectra of detrital zircons in Lhasa, Nianchu and Pumchu river sands (insets show ages < 300 Ma in greater detail). Kernel density estimate plots after Vermeesch (2012).

grains are associated with carbonate, minor gneiss, and rare metabasite rock fragments. Micas are few. The moderately rich transparent-heavy-mineral assemblage contains diopsidic clinopyroxene, blue-green to green-brown amphibole, tourmaline, epidote, garnet, minor zircon, apatite, titanite, and rutile.

6. Detrital geochronology

6.1. Detrital zircon

For each sample, between 100 and 115 usable U−Pb ages ranging from 7 Ma to 3 Ga (Fig. 4) were obtained from zircon grains 50–150 μm in diameter. Detrital zircons are mostly euhedral to subhedral in Lhasa River sand, whereas they are mostly rounded to well-rounded in Nianchu and Pumchu sands. In Lhasa River sand, U−Pb ages cluster at 7–22 Ma (6%), 28–66 Ma (70%, peak ~46.5 Ma), 75–199 Ma (10%, peak ~138 Ma), 456–833 Ma (10%, peak ~567 Ma), 1117–1784 Ma (4%, peak ~1453 Ma). In Nianchu sand, U−Pb ages cluster at 53–131 Ma (6%, peak ~90 Ma), 404–589 Ma (36%, peak ~502 Ma), 808–1605 Ma (41%, peak ~910 Ma), 2479–2820 Ma (17%, peak ~2580 Ma). The age distribution is similar in Pumchu sand, where U−Pb ages cluster at 400–707 Ma (46%, peak ~496 Ma), 800–978 Ma (28%, peak ~831 Ma), 1188–1882 Ma (15%, peak ~1760 Ma), and 2121–2621 Ma (11%, peak ~2629 Ma).

The Th/U ratio is generally > 0.1 for magmatic zircon and < 0.1 for metamorphic zircon (Hartmann and Santos, 2004), and can thus be used as a provenance tracer. All grains in Lhasa River sand have Th/U > 0.1 but for one grain dated as ~55 Ma (Fig. 5), indicating dominance of magmatic zircons. A few more grains with Th/U < 0.1, occur in Nianchu (five grains dated between 670 and 1200 Ma) and Pumchu sands (two grains dated around 500 Ma), suggesting metamorphic provenance, although 95–98% of zircon grains show magmatic provenance with Th/U > 0.1.

6.2. Detrital monazite

For each sample, between 108 and 120 usable U-Th-Pb ages ranging from 8 Ma to 1.5 Ga (Fig. 4) were obtained from monazite grains 100–200 μm in diameter. In Lhasa River sand, U-Th-Pb ages cluster at 8–13 Ma (50%, peak ~10 Ma), 14–34 Ma (32%, peak ~20 Ma), 50–89 Ma (12%, peak ~64 Ma), 102–202 Ma (6%, peak ~161 Ma). In Nianchu sand, U-Th-Pb ages cluster at 11–19 Ma (20%, peak ~15 Ma), 20–28 Ma (39%, peak ~22 Ma), 32–68 Ma (8%, peak ~40 Ma), 430–590 Ma (24%, peak ~487 Ma), 804–1172 Ma (9%, peak

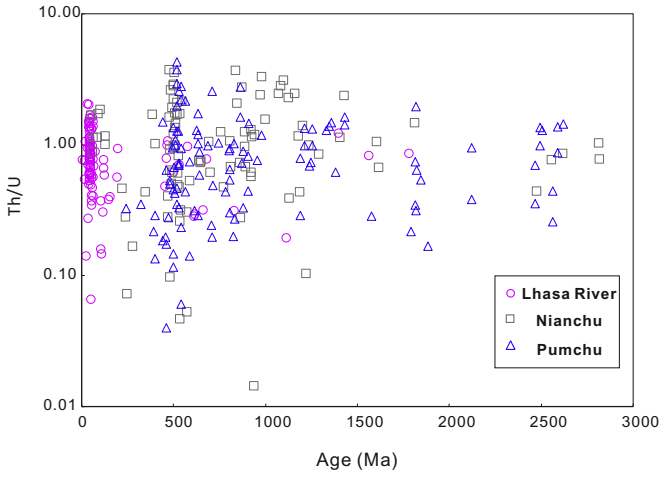

Fig. 5. U–Pb age vs. Th/U plot of detrital zircons in in Lhasa, Nianchu, and Pumchu river sands.

~887 Ma). The age distribution is similar in Pumchu sand, where U-Th-Pb ages cluster at 11–17 Ma (22%, peak ~14 Ma), 18–22 Ma (40%, peak ~20 Ma), 23–46 Ma(17%, peak ~25 Ma), 321–579 Ma (18%, peak ~521 Ma).

Monazite, commonly occurring in granite, gneiss, schist, and granulite, is rich in Th, U, and light rare earth elements (LREEs; Williams et al., 2007). All of the analysed monazite grains from the Lhasa River, Nianchu, and Pumchu show strong LREE enrichment and steep right-obliqueREE pattern (Fig. 6). The magmatic or metamorphic source of detrital monazite cannot be robustly discriminated by the lanthanide element tetrad-effect (Qiu and Yang, 2011; Liu et al., 2016), and the analysed monazite grains plot in the area of the Sm/Nd-La/Yb diagram where magmatic and metamorphic rocks overlap (Fig. 7). The combination of other geochemical parameters such as $[Gd/Lu]_N$, Eu/Eu*, and $[Th/U]_N$ can be used to this purpose (Itano et al., 2016). Metamorphic monazites tend to have $[Gd/Lu]_N > 500$ or Eu/Eu* < 0.2 and $[Th/U]_N > 20$ if $[Gd/Lu]_N < 500$. Magmatic monazites tend to have $[Gd/Lu]_N < 500$, Eu/Eu* < 0.2, and $[Th/U]_N > 20$. Grains with $[Gd/Lu]_N < 500$, Eu/Eu* < 0.2 and $[Th/U]_N < 20$ are undecided.

All monazite grains in Lhasa River sand yielded $[Gd/Lu]_N < 500$, all but one $[Th/U]_N < 20$, and 93% Eu/Eu* < 0.2. In Nianchu sand, 90% yielded $[Gd/Lu]_N < 500$, 94% have $[Th/U]_N < 20.7$, and 67% Eu/Eu* < 0.2. In Pumchu sand, 93% yielded $[Gd/Lu]_N < 500$, 98% have $[Th/U]_N < 20$, and 63% Eu/Eu* < 0.2. These results do not allow a clear provenance diagnosis for most monazite grains, but they do indicate a sharp difference between Lhasa River sand, where grains are either undecided or magmatic, versus Nianchu and Pumchu sands, where grains are either undecided or metamorphic.

6.3. Detrital titanite

For each sample, between 100 and 117 usable U–Pb ages mostly ranging from 3 Ma to ~300 Ma were obtained (Fig. 4). Detrital titanites are larger than 200 μm in diameter, clear, and mostly euhedral in Lhasa River sand, whereas they are commonly smaller than 200 μm, well rounded and display frosted surfaces in Nianchu and Pumchu sands.

In Lhasa River sand, U–Pb ages cluster at 7–21 Ma (4.4%, peak ~12.5 Ma), 24–57 Ma (88%, peak ~50 Ma), and 66–101 Ma (7.6%, peak ~84 Ma). In Nianchu sand, U–Pb ages cluster at 3–44 Ma (77%, peak ~22 Ma), 50–154 Ma (14%, peak ~128 Ma), and 192–980 Ma (10%, peak ~494 Ma). In Pumchu sand, U–Pb ages cluster at 7–40 Ma (96%, peak ~23 Ma) and 102–847 Ma (4%, peak ~282 Ma).

Titanite is a Ca-rich silicate mineral commonly found in both igneous rocks including diorite and granodiorite and in metamorphic rocks including calc-silicates and marbles. Provenance of detrital

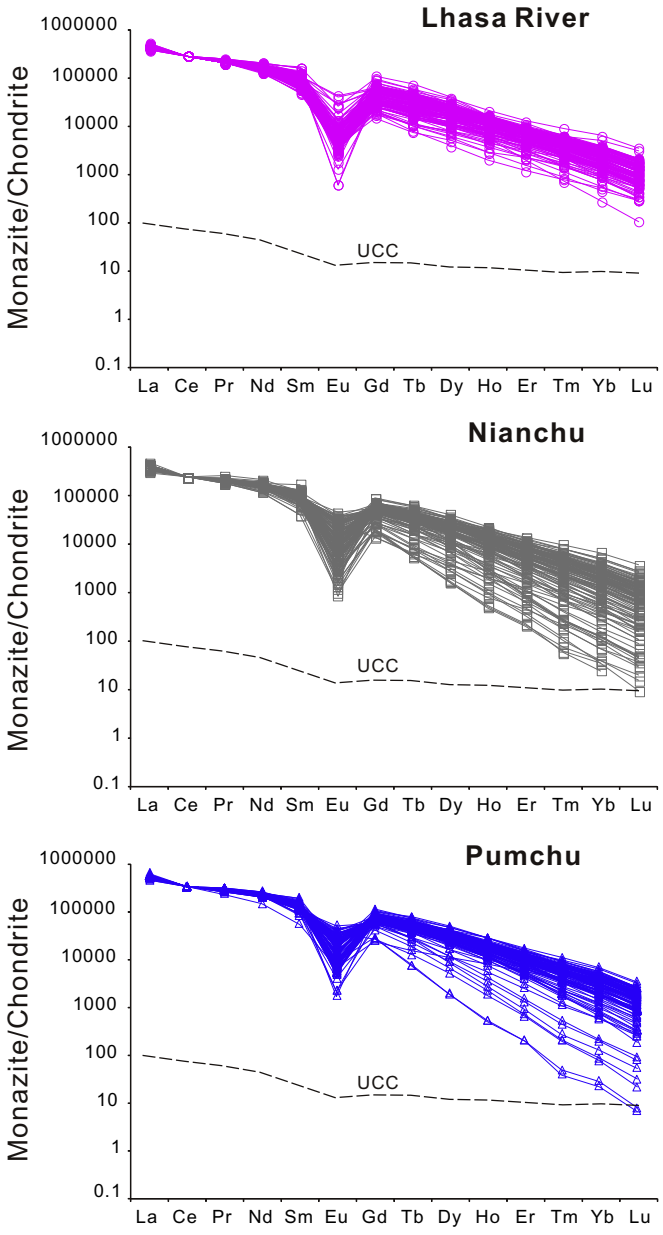

Fig. 6. Chondrite-normalized REE patterns of detrital monazite in Lhasa, Nianchu, and Pumchu river sands (chondrite values used for normalization after Sun and McDonough, 1989; Upper Continental Crust standard after Rudnick and Gao, 2003).

titanite may be discriminated by using the Th/U, LREE/HREE, and Nb/Ta ratios (Mazdab et al., 2007; Gao et al., 2012; Fu et al., 2016;). Magmatic titanite tends to have right-oblique REE pattern and Th/U > 1, whereas metamorphic or hydrothermal titanite tends to have relatively flat REE distribution and Th/U < 1.

In detrital titanite from Lhasa River sand, LREEs are slightly enriched and HREEs slightly depleted (Fig. 8) (LREE/HREE from 2.3 to 47, average 17; Ce/Ce* from 0.97 to 1.28, average 1.16; Eu/Eu* from 0.17 to 2.7, average 1.02). the Th/U ratio ranges from 0.2 to 16 (average 5.9; 93% of grains with Th/U > 1; Fig. 9A) and the Nb/Ta ratio from 3.9 to 257 (average 27.5; Fig. 9B).

In detrital titanite from Nianchu and Punchu sands, both LREE and HREE patterns are rather flat (LREE/HREE from 0.05 to 8.7, average 2.4 and 2.6; Fig. 8), in Nianchu sand, Ce/Ce* ranges from 0.3 to 2.3 (average 0.74) and Eu/Eu* from 0.95 to 1.64 (average 1.18), in Pumchu sand, Ce/Ce* ranges from 0.1 to 1.2 (average 0.63) and Eu/Eu*

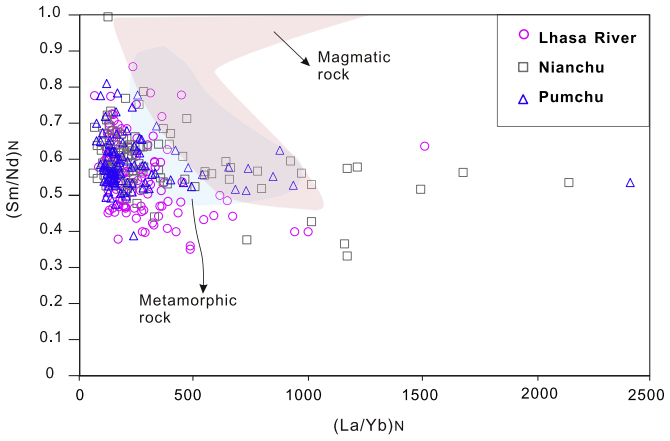

Fig. 7. (Sm/Nd)N vs. (La/Yb)N plot for detrital monazite in Lhasa, Nianchu, and Pumchu river sands (data on magmatic and metamorphic rocks after Liu et al., 2016; chondrite values used for normalization after Sun and McDonough, 1989).

from 1.06 to 1.34 (average 1.16). The Th/U ratio ranges from 0.04 to 4.8; respectively 67% and 70% of grains yielded Th/U < 1 (Fig. 9). These data suggest a magmatic origin for > 90% of titanite grains in Lhasa River sand, and an ultimate metamorphic origin for ~70% of titanite grains in Nianchu and Pumchu sands.

6.4. Detrital rutile

For each sample, between 88 and 118 usable U–Pb ages were obtained from rutile grains 100–200 μm in diameter. In Lhasa River sand, U–Pb ages cluster at 8–33 Ma (14%, peak ~13 Ma), 40–73 Ma (11%, peak ~57 Ma), 98–200 Ma (42%, peak ~145 Ma), 489–758 (20%, peak ~529 Ma), and 861–1590 (11%, peak ~952 Ma) (Fig. 4). In Nianchu sand, U–Pb ages cluster at 480–662 Ma (96%, peak ~500 Ma) with three grains yielding U–Pb ages of 15–16 Ma (4%). In Pumchu sand, U–Pb ages cluster at 8–27 Ma (26%, peak ~16 Ma), 440–675 Ma (72%, peak ~550 Ma), and 800–980 Ma (2%, peak ~912 Ma) (Fig. 4).

Rutile occurs mainly in medium- to high-pressure metamorphic rocks, including metapelite and metabasite, and only rarely in magmatic rocks (Zack, 2017). The Cr/Nb ratio is widely used as a provenance tracer, being higher in rutile from mafic rocks and lower in rutile from metapelite (Zack et al., 2004; Triebold et al., 2007, 2012; Meinhold et al., 2008; Meinhold, 2010). Here, we utilize the parameter X proposed by Triebold et al., 2012 for lithological discrimination, where.

$$X = 5 * (Nb_{ppm} - 500) - Cr_{ppm}$$

If X < 0, then the source is likely to be a metabasite, whereas if X > 0 it is likely to be a metapelite. X is > 0 for 95%, 89%, and 97% of grains in Lhasa River, Nianchu, and Pumchu sands, respectively, suggesting provenance mostly from metapelite in all three cases (Fig. 10). X is < 0 for two grains in Lhasa River sand yielding U–Pb ages of 52 and 116 Ma.

7. Magmatic and metamorphic events reflected in detrital minerals

7.1. Detrital zircon

In litho-feldspatho-quartzose Lhasa River sand (Fig. 3), which includes common granitoid, volcanic and sedimentary to low-rank metasedimentary rock fragments, zircon grains are mostly euhedral to subhedral and their geochemical signatures suggest a magmatic origin for most (Fig. 5). Paleogene ages are dominant (70%) (Fig. 4), broadly

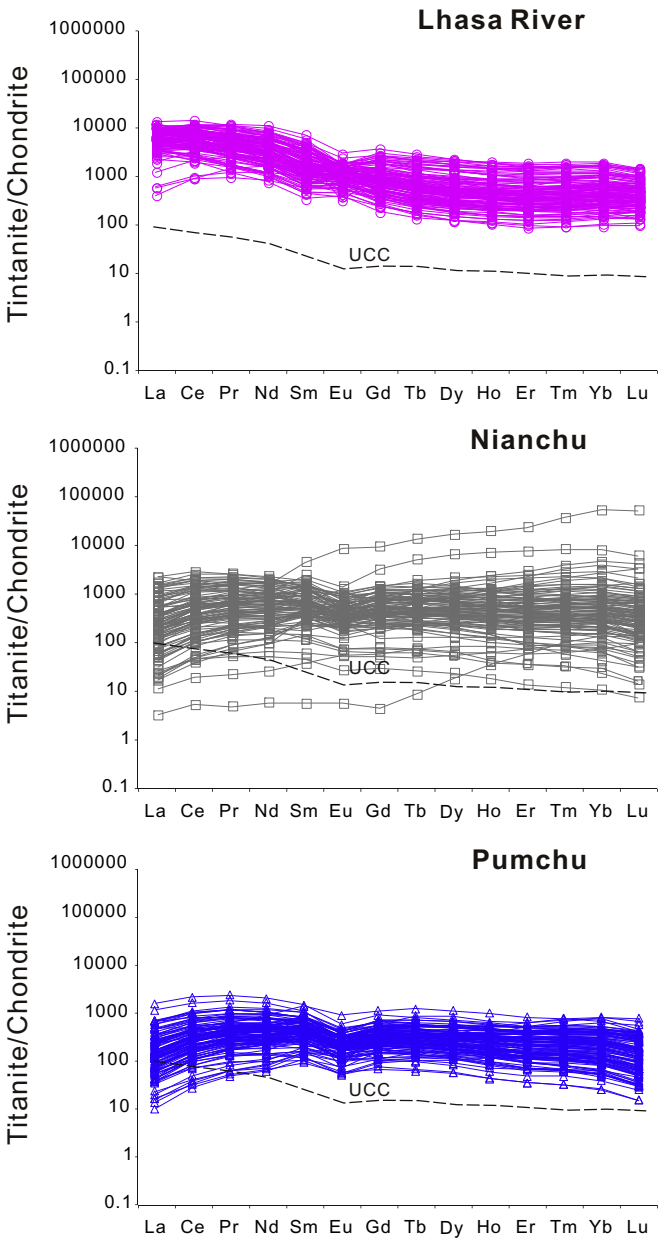

Fig. 8. Chondrite-normalized REE patterns for detrital titanites in Lhasa, Nianchu, and Pumchu river sands (chondrite values used for normalization after Sun and McDonough, 1989; Upper Continental Crust standard after Rudnick and Gao, 2003).

matching the time of magmatic flare-up in the Gangdese arc (Fig. 11A) (Zhu et al., 2015). A few Miocene zircons (6%) were probably derived from the Nyainqentanglha Range, whereas Jurassic and Cretaceous ages (10%) suggest provenance from granitoid intrusions in the central and northern Lhasa block (Figs. 2, 4). The latest Proterozoic-early Paleozoic and mid-Proterozoic age clusters (14% overall) coincide with those obtained from very-low-grade Carboniferous-Permian metasedimentary rocks that are widespread in the central Lhasa block (Leier et al., 2010) (Figs. 2, 4). The high Th/U ratio yielded by all grains but one confirms dominantly magmatic provenance (Fig. 5).

In feldspatho-quartzo-lithic Nianchu and feldspatho-litho-quartzose Pumchu sands (Fig. 3), both dominated by shale/slate and siltstone/metasiltstone lithics and containing a few granitoid, schistose and gneissic rock fragments, zircon grains are mostly rounded, indicating that they are largely recycled from siliciclastic rocks of the Tethys Himalaya (Fig. 2). U–Pb age-spectra show peaks in the Cambrian

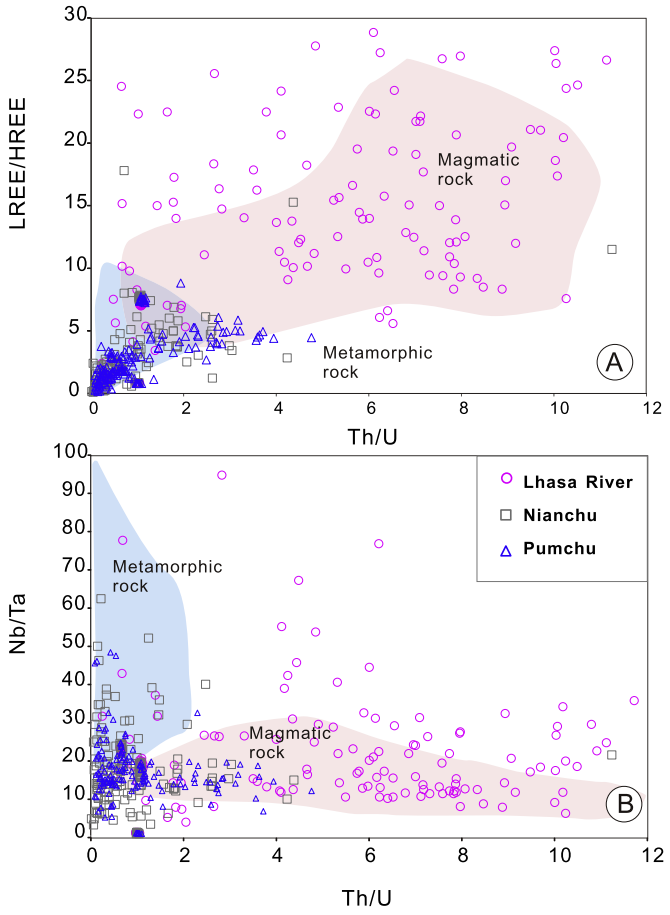

Fig. 9. LREE/HREE vs. Th/U plot (A) and Nb/Ta vs.Th/U plot (B) for detrital titanites in Lhasa, Nianchu, and Pumchu river sands (data on magmatic and metamorphic bedrocks after Fu et al., 2016).

(36–46%), early Neoproterozoic (41–28%), and Neoarchean (17–11%) (Figs. 2, 4), consistently with geochronological data previously obtained from Tethys Himalayan and Greater Himalayan rocks (Fig. 11B, C, D) (Gehrels et al., 2011). Nianchu sand also yielded a few grains (6%) with Cretaceous to Paleogene ages, possibly derived from the Northern Himalayan Kangmar gneiss dome, whereas Pumchu sand shows an additional Paleoproterozoic cluster at ~1.8 Ga (15%), which suggests ultimate provenance from Indian basement rocks (Figs. 2, 4). Ultimate provenance from metamorphic rocks is suggested for several grains characterized by low Th/U ratio (Fig. 5).

7.2. Detrital monazite

Oligo-Miocene U-Th-Pb ages are dominant in Lhasa River sand, in the same range as monazites in granite, orthogneiss, and mylonite of the Nyainqentanglha Range (13–28 Ma; Xu et al., 1985; Kapp et al., 2005; Figs. 2, 4). Subordinate Eocene to Cretaceous and Jurassic ages may be derived from granitoid rocks of the southern, central, and northern Lhasa block (Figs. 2, 4).

U-Th-Pb ages ranging between the late Eocene and the Miocene are dominant also in Nianchu and Pumchu sands (Fig. 4), reflecting the timing of magmatic or metamorphic growth of monazite in Greater Himalayan leucogranites and gneisses. Geochemical fingerprints are of little help to effectively discriminate between monazite grains of magmatic or metamorphic provenance (Figs. 6, 7).

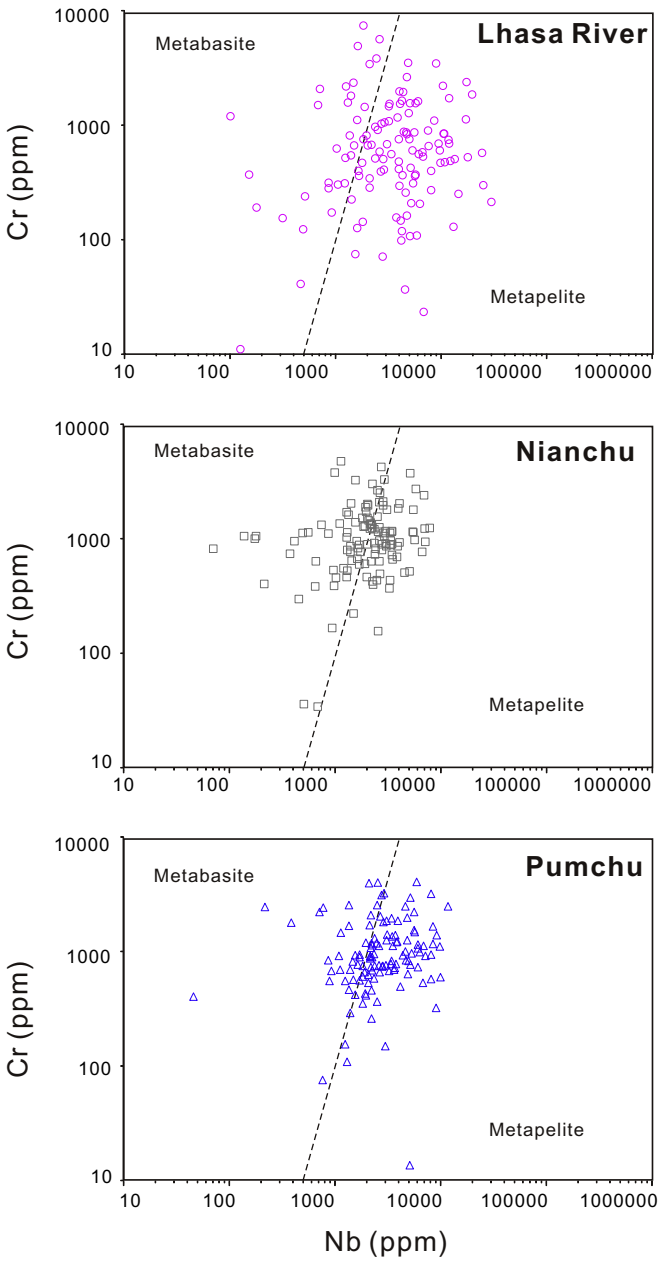

Fig. 10. Provenance of detrital rutiles in the Lhasa, Nuianchu and Pumchu river sands discriminated by the Cr vs. Nb diagram (after Triebold et al., 2012).

7.3. Detrital titanite

Detrital titanite in Lhasa River sand yielded mostly Eocene-Oligocene U—Pb ages and some Late Cretaceous ages (Fig. 4), suggesting provenance from the Gangdese arc and reflecting both post-collisional and pre-collisional magmatic activity. I-type granites dated around 50 Ma characterize the southern Lhasa terrane (Zhang et al., 2012), whereas titanites yielding Jurassic ages were reported from granitoid bodies in both the southern Lhasa and northern Ando terranes, considered as generated during the India-Asia and Lhasa-Qiangtang collisions, respectively (Xu et al., 1985; Xie et al., 2018). The few Miocene grains were possibly derived from intrusive and metamorphic rocks of the Nyainqentanglha Range (Figs. 2, 4). The magmatic origin of most titanite grains is confirmed by their large size, clear surface, and euhedral shape.

The geochemical signatures of generally smaller and rounded titanite grains found in Nianchu and Pumchu sands indicate instead a

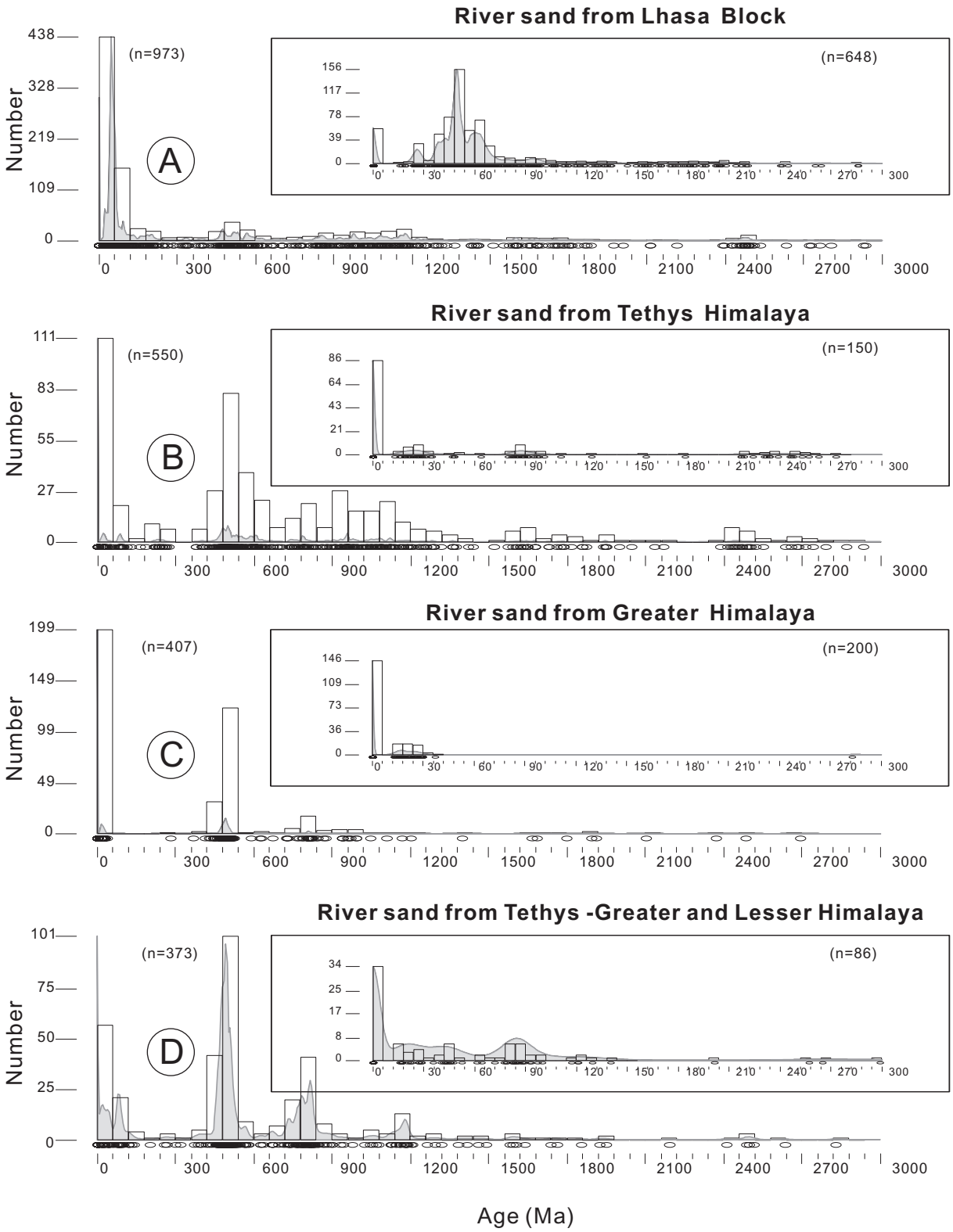

Fig. 11. U–Pb age spectra of detrital zircons in modern river sands derived from the Lhasa Block (A; Cina et al., 2009; Zhang et al., 2012; Bracciali et al., 2015; Ji et al., 2016; Carrapa et al., 2017), the Tethys Himalaya (B; Zhang et al., 2012; Bracciali et al., 2016; Carrapa et al., 2017), the Greater Himalaya (C; Bracciali et al., 2015), and diverse domains of the Himalayan orogen (D; Cina et al., 2009; Bracciali et al., 2016). Kernel density estimate plots after Vermeesch (2012).

largely metamorphic origin (Figs. 8, 9). Their ages mostly range from 3 to 44 Ma with peak at 22–23 Ma, thus reflecting the main stage of metamorphic evolution in the Greater Himalayan domain (Figs. 2, 4). Metamorphic growth of titanite is documented to have taken place between 13 and 20 Ma in high-temperature calc-silicates exposed in the Pumchu basin near Kada (Cottle et al., 2011), and between 12 and 30 Ma in amphibolites and calc-silicate gneisses all along the Greater Himalaya from northwest India to Bhutan (Mottram et al., 2018). Gabbros yielding titanite dated as 45 Ma are exposed close to the eastern watershed of the Nianchu (Ji et al., 2016). Titanites yielding

older ages reflect earlier magmatic events that took place in the Early Cretaceous, Permian, and Cambrian (Garzanti et al., 1986, 1999; Hu et al., 2010).

7.4. Detrital rutile

The geochemical fingerprint of most rutile grains in three river catchments point to metapelitic source rocks (Fig. 10). Young (8–33 Ma) Oligo-Miocene grains in Lhasa River sand indicate provenance from the Nyainqentanglha Range (Xu et al., 1985; Kapp et al., 2005; Ji et al., 2009; Dong et al., 2011; Figs. 2, 4). Most grains, however, yielded Early Cretaceous to Jurassic ages and some Cambrian to Mesoproterozoic ages suggesting mixed contributions from the Nyainqentanglha Range and other pre-Cenozoic metasedimentary rocks (Figs. 2, 4).

Most rutile grains in Nianchu and Pumchu sands yielded Ordovician to late Neoproterozoic ages, the mark of the Pan-African orogenic event widely documented at the core of Northern Himalayan domes and in the Tethys Himalayan and Greater Himalayan domains (Garzanti et al., 1986; DeCelles et al., 2000; Lee et al., 2000; Figs. 2, 4). The amount of young Miocene grains (Fig. 4), rare in Nianchu sand and more common in Pumchu sand, is only very roughly proportional to areal exposures of metamorphic rocks (4% vs. 2.2% and 26% vs. 9.5%, respectively).

7.5. Summary

Detrital zircon, monazite, titanite and rutile respond differently to magmatic and metamorphic events recorded in each river catchment:

1) Lhasa river: the unimodal age peak at ~52 Ma displayed by detrital zircon and titanite carried by the Lhasa River reflect prominent Gangdese arc magmatism in the southern Lhasa terrane (Fig. 12). Instead, rutile and monazite reveal the post-collision metamorphic event (8–33 Ma) affecting the Nyainqentanglha Range, an event which has not been recognized for long (Fig. 12);
2) Nianchu and Pumchu: detrital monazite is chiefly derived from the leucogranite bodies exposed locally in the Nianchu and Pumchu headwaters. Detrital titanite, instead, mostly reflects metamorphic events, which ranged in age from 44 to 3 Ma along the northern flank of the Himalayan range (Fig. 13);
3) detrital zircon and rutile respond poorly to such young events, and display spectra dominated by Early Paleozoic (> 500 Ma) and older Precambrian ages (Figs. 12, 13).

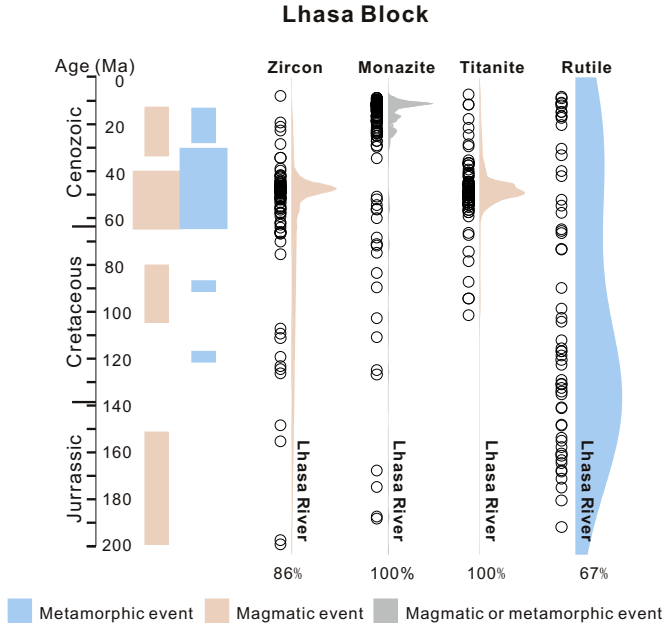

Fig. 12. Main magmatic and metamorphic events of crustal growth that took place in the Lhasa Block in the last 200 Ma, as reflected by geochronological ages of detrital zircon, monazite, titanite, and rutile. Percentages indicate the proportion of grains younger than 200 Ma for each mineral. The pink and blue areas outline the main magmatic and metamorphic events that took place in the Lhasa Block (Ji et al., 2009; Zhu et al., 2011, and Zhang et al., 2014). (For interpretation of the references to colour in this figure legend, the reader is referred to the web version of this article.)

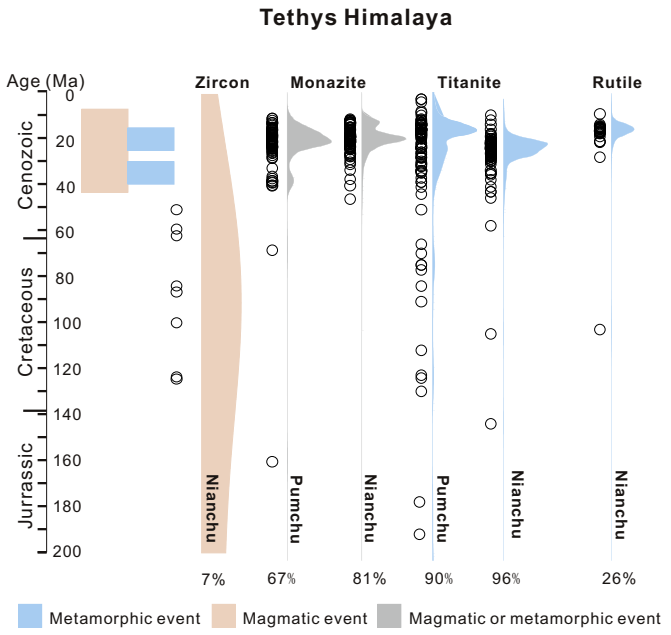

Fig. 13. Main magmatic and metamorphic events of crustal growth that took place in the Tethys Himalaya during the last 200 Ma, as reflected by geochronological ages of detrital zircon, monazite, titanite, and rutile. Percentages indicate the proportion of grains younger than 200 Ma for each mineral. The pink and blue areas outline the main magmatic and metamorphic event that affected the Tethys Himalaya (Ji et al., 2009; Zhu et al., 2011, and Zhang et al., 2014). (For interpretation of the references to colour in this figure legend, the reader is referred to the web version of this article.)

This indicates that durable zircon and rutile grains have largely survived more than a single sedimentary cycle and are largely recycled from widely exposed Tethys Himalayan siliciclastic rocks, whereas monazite and titanite grains are mostly derived from first-cycle crystalline bedrock.

8. Implications for quantitative provenance analysis

In recent years, age-spectra of detrital zircon and other minerals have been tentatively used to constrain sediment budgets and quantify erosion rates within a river catchment (Stock et al., 2006; Rahl et al., 2007; Carrapa, 2009; Zhang et al., 2016). Some studies found that the age distribution of detrital zircons may accurately reflect mixing in proportions roughly corresponding to the extent of the areal exposure of their parent rocks, and thus concluded that the relative exposure areas of contributing sources can be estimated approximately from detrital-zircon age data (Saylor et al., 2013). Other researchers, however, showed that the fertility of target minerals may vary by orders of magnitudes among source rocks, and therefore proportional contributions from different sources should not be expected (Moecher and Samson, 2006; Dickinson, 2008; Malusà and Garzanti, 2019). The potential pitfalls involved in the calculation of sediment budgets based on single-mineral data have been discussed and highlighted in Vezzoli et al. (2016b). In the Tibetan region, Carrapa et al. (2017) compared

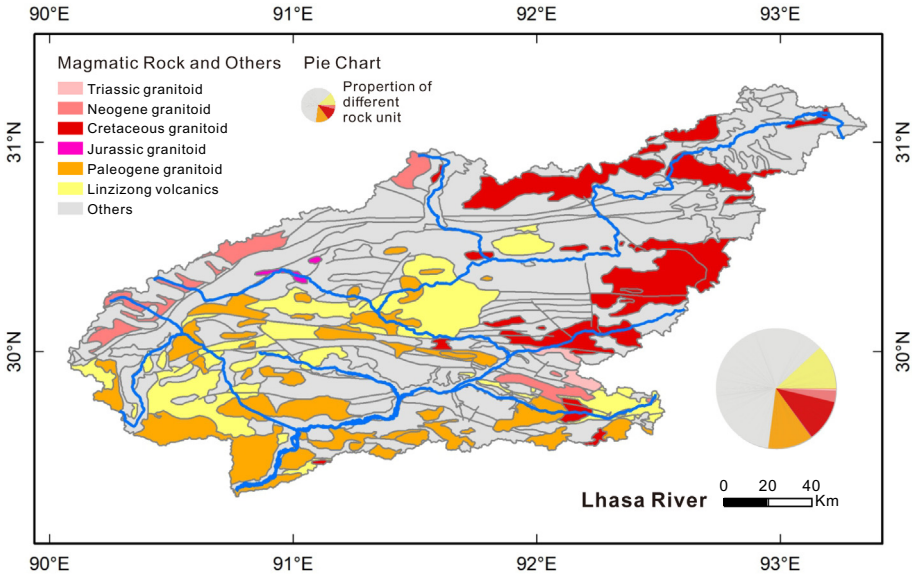

Fig. 14. Areal exposure of Jurassic, Cretaceous, Paleogene, and Neogene magmatic rocks in the Lhasa river catchment.

the percentage of zircons grains yielding ages between 40 and 120 Ma in seven tributaries of the Yarlung Tsangpo - six draining the suture zone and Lhasa block in the north and one draining the Tethys Himalaya in the south - with the areal exposures of Gangdese arc rocks in each catchment, finding a strong positive correlation ($R^2 = 0.81$).

Our ArcGIS calculations indicate that the area of the Lhasa River, Nianchu, and Pumchu catchments amount, respectively, to 32,632 km^2, 11,113 km^2, and 25,573 km^2, of which 12,663 km^2 (~39%), 266 km^2 (~3%) and 1022 km^2 (~4%) represented by igneous rocks (Fig. 2). The corresponding percentages of detrital-zircon ages < 120 Ma, however, are 74%, 7%, and 0% respectively (Fig. 15A) indicating a poor relationship between the distribution of zircon ages and areal exposures of corresponding intrusive rocks. Such a poor proportional relationship is also apparent for data in Carrapa et al. (2017) for their rivers R3, R4, R5, and R7.

This issue, crucial to validate the use of single-mineral data in the calculation of sediment budgets, can be investigated in greater detail in the Lhasa River catchment, where the areal exposure of the Jurassic, Cretaceous, Paleogene, and Neogene granitoids is 0.3%, 11.3%, 12.4%, and 3.1% respectively (Fig. 14). Linzizong volcanic rocks, not considered in Carrapa et al. (2017), represent 12.2% (Fig. 14). The areal exposure of Paleogene plutonic and volcanic rocks is about twice as that of Cretaceous plutonic rocks, but Paleogene zircon grains (34–65 Ma) represent as much as 70%, and Cretaceous grains (66–145 Ma) only 13% of total detrital zircons (Fig. 15B). The titanite budget is even more unbalanced: 88% of grains yielded ages between 24 and 57 Ma, whereas only 7.8% of titanite grains yielded Cretaceous ages (66–101 Ma) (Fig. 15C). The zircon and titanite generation potential (fertility) of Paleogene igneous rocks is greater than that of Cretaceous plutonic rocks by factors of ~2.5 and ~5. Moreover, Neogene plutonic rocks account for a mere 3% of the river catchment, and yet they are able to produce as much as 72% of monazite grains (Fig. 15D).

The main causes of such even large differences observed between the areal extent of bedrock exposures and relative abundance of a single mineral, or of a single age population, are mineral fertilities, which may vary by orders of magnitude (Moecher and Samson, 2006; Malusà et al., 2016), and different erosion rates, which also may vary by one order of magnitude or more. The latter factor is dependent in turn on tectonic activity, geomorphic features (e.g., topography and relief; Zhang et al., 2012; Jonell et al., 2017), and climate (e.g., amount and seasonal distribution of rainfall and frequency of catastrophic events including floods and landslides; Lang et al., 2013; Jonell et al., 2017).

Geomorphic and climatic conditions are relatively easy to assess in modern settings (e.g., from the Shuttle Radar Topography Mission SRTM and Tropical Rainfall Measuring Mission TRMM databases). The concentration (fertility) of single minerals in specific source rocks, instead, is much harder to evaluate even grossly, and requires not only detailed mineralogical and/or geochemical data on either numerous and statistically representative bedrock samples or carefully selected sediment samples that can be considered as not significantly affected by hydraulic-sorting processes (Garzanti and Andò, 2019). Geochemical analyses offer a particularly straightforward means to measure zircon and possibly also monazite fertility in crystalline bedrock, which can be roughly considered as directly proportional to the concentration of Zr and LREEs, respectively (Dickinson, 2008). However, peralkaline igneous rocks can incorporate wt% Zr without crystallising zircon (Watson, 1979), and other phases such as apatite, monazite, allanite and clay minerals can also host wt% ΣREEs. Information on rutile and titanite, however, cannot be obtained with the same robustness, because there are other major carriers of titanium (e.g., ilmenite). In the Himalayan and Tibetan study area we are very far from disposing of adequate information on the fertility of our targeted mineral groups in all potential source rocks, and erosion rates in different geological domains, rather than known, represent the unknown of the equation we want to contribute solving (e.g., Garzanti et al., 2019).

In summary, this weak positive correlation between the areal exposure of granitoids of different ages and their ability to generate zircon, titanite, and monazite grains confirms that age distributions of single minerals cannot be used reliably in the calculation of sediment budgets, although they do provide essential information in qualitative provenance reconstructions.

9. Conclusions

The geochronological and geochemical fingerprints of detrital zircon, monazite, titanite, and rutile were used in this study to highlight the potential and limitations of the use of single-mineral methods for qualitative and quantitative provenance analysis. Our data show that different heavy minerals reflect the areal distribution of magmatic and metamorphic source rocks differently, and conclude that advanced single-mineral approaches do provide fundamental provenance information but cannot be used reliably in quantitative provenance reconstructions.

Detrital zircon is a good tracer but chiefly only for granitoid and

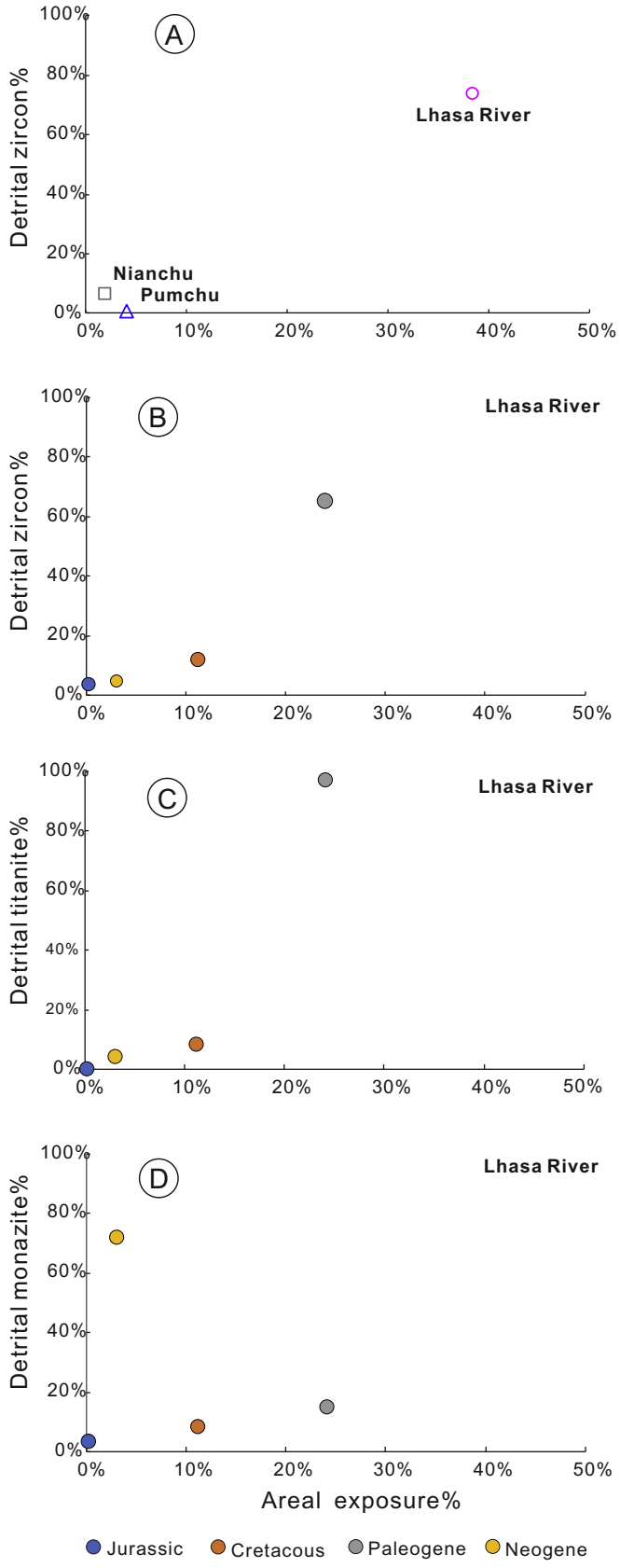

Fig. 15. Comparison between areal exposures and percentages of detrital minerals of corresponding ages. A) Areal exposures of magmatic rocks younger than 120 Ma vs. percentages of detrital zircons younger than 120 Ma in Lhasa, Nianchu, and Pumchu river sands. Percentages of zircon (B), titanite (C), and monazite grains (D) in Lhasa River sand compared with areal exposure of Jurassic, Cretaceous, Eocene and Paleogene magmatic rocks in the Lhasa River

volcanic source rocks, whereas rutile grains convey information mostly limited to the metapelite or metabasite nature of their parent rocks. The geochemical signature of titanite grains allows distinction between their magmatic versus metamorphic origin, which is hardly the case for detrital monazite. A complete panorama on source rocks and on erosion patterns, therefore, can only be achieved by integrating analyses of the bulk sediment sample with the results obtained from a spectrum of different mineral groups, which justifies the rationale of the present study. As a final example to emphasize this central issue, our data indicate that the age distributions of different detrital minerals in Lhasa River sand do record the different magmatic events in the catchment, but the correlation between areal exposures and percentages of corresponding detrital-mineral ages is poor for zircon, very poor for titanite, and extremely poor for monazite. These results cast shadows on the use of single-mineral data in the calculation of sediment budgets and inferences on erosion patterns, unless the composition of the bulk sediment together with a spectrum of different mineral groups are taken into due account and differences in mineral fertilities are accurately determined.

Declaration of Competing Interest

The authors declare that they have no known competing financial interests or personal relationships that could have appeared to influence the work reported in this paper.

Acknowledgments

We thank Juan Li, Zhong Han, Wei An, Hanpu Fu and Anlin Ma for their assistance in the field, and Yueheng Yang, Bing Wu, Jiangang Wang and Xiaochi Liu for their fundamental help in geochronological analyses. Petrographic and heavy-mineral analyses were performed by Giovanni Vezzoli, Mara Limonta, and Wendong Liang at the Laboratory for Provenance Studies at the University of Milano-Bicocca. This study was financially supported by the Second Tibetan Plateau Scientific Expedition and Research Program (STEP), Ministry of Science and Technology, China (2019QZKK0204).

References

Aikman, A.B., Harrison, T.M., Lin, D., 2008. Evidence for early (> 44Ma) Himalayan Crustal Thickening, Tethyan Himalaya, southeastern Tibet. Earth Planet. Sci. Lett. 274 (1), 14–23.

Aleinikoff, J.N., Wintsch, R.P., Fanning, C.M., Dorais, M.J., 2002. U–Pb geochronology of zircon and polygenetic titanite from the Glastonbury complex, Connecticut, USA: an integrated SEM, EMPA, TIMS, and SHRIMP study. Chem. Geol. 188 (1), 125–147.

Andersen, T., 2002. Correction of common lead in U–Pb analyses that do not report 204Pb. Chem. Geol. 192 (1), 59–79.

Andersen, T., 2005. Detrital zircons as tracers of sedimentary provenance: limiting conditions from statistics and numerical simulation. Chem. Geol. 216 (3), 249–270.

Belousova, E., Griffin, W., O'Reilly, S.Y., Fisher, N., 2002. Igneous zircon: trace element composition as an indicator of source rock type. Contrib. Mineral. Petrol. 143 (5), 602–622.

Black, L.P., Gulson, B.L., 1978. The age of the Mud Tank carbonatite, Strangways Range, Northern Territory. BMR J. Aust. Geol. Geophys. 3, 227–232.

Bracciali, L., Parrish, R.R., Horstwood, M.S.A., Condon, D.J., Najman, Y., 2013. U-Pb LA-(MC)-ICP-MS dating of rutile: new reference materials and applications to sedimentary provenance. Chem. Geol. 347 (4), 82–101.

Bracciali, L., Najman, Y., Parrish, R.R., Akhter, S.H., Millar, I., 2015. The Brahmaputra tale of tectonics and erosion: early Miocene river capture in the Eastern Himalaya. Earth Planet. Sci. Lett. 415, 25–37.

Bracciali, L., Parrish, R.R., Najman, Y., Smye, A., Carter, A., Wijbrans, R., 2016. Plio-Pleistocene exhumation of the eastern Himalayan syntaxis and its domal pop-up. Earth Sci. Rev. 160, 350–385.

Buick, I.S., Clark, C., Rubatto, D., Hermann, J., Pandit, M., Hand, M., 2010. Constraints on the Proterozoic evolution of the Aravalli-Delhi Orogenic belt (NW India) from monazite geochronology and mineral trace element geochemistry. Lithos 120 (3), 511–528.

Carosi, R., Montomoli, C., Iaccarino, S., 2018. 20 years of geological mapping of the metamorphic core across Central and Eastern Himalayas. Earth-Sci. Rev. 177, 124–138.

Carrapa, B., 2009. Tracing exhumation and orogenic wedge dynamics in the European Alps with detrital thermochronology. Geology 37 (12), 1127–1130.

Carrapa, B., 2010. Resolving tectonic problems by dating detrital minerals. Geology 38 (2), 191–192.
Carrapa, B., Hassim, M.F.B., Kapp, P.A., Decelles, P.G., Gehrels, G., 2017. Tectonic and erosional history of southern Tibet recorded by detrital chronological signatures along the Yarlung River drainage. Geol. Soc. Am. Bull. B31587, 1.
Carroll, D., 1953. Weatherability of zircon. J. Sediment. Res. 23 (2), 106–116.
Cawood, P.A., Hawkesworth, C.J., Dhuime, B., 2012. Detrital zircon record and tectonic setting. Geology 40 (10), 875–878.
Chew, D.M., Sylvester, P.J., Tubrett, M.N., 2011. U–Pb and Th–Pb dating of apatite by LA-ICPMS. Chem. Geol. 280 (1), 200–216.
Chew, D.M., Petrus, J.A., Kamber, B.S., 2014. U–Pb LA–ICPMS dating using accessory mineral standards with variable common Pb. Chem. Geol. 363, 185–199.
Chu, M.F., Chung, S.L., Song, B., Liu, D., O'Reilly, S.Y., Pearson, N.J., Ji, J.Q., Wen, D.J., 2006. Zircon U-Pb and Hf isotope constraints on the Mesozoic tectonics and crustal evolution of southern Tibet. Geology 34 (9), 745–748.
Chung, S.L., Chu, M.F., Zhang, Y.Q., Xie, Y.W., Lo, C.H., Lee, T.Y., Lan, C.Y., Li, X.H., Zhang, Q., Wang, Y.Z., 2005. Tibetan tectonic evolution inferred from spatial and temporal variations in post-collisional magmatism. Earth-Sci. Rev. 68 (3), 173–196.
Cina, S.E., Yin, A., Grove, M., Dubey, C.S., Shukla, D.P., Lovera, O.M., Kelty, T.K., Gehrels, G.E., Foster, D.A., 2009. Gangdese arc detritus within the eastern Himalayan Neogene foreland basin: implications for the Neogene evolution of the Yalu–Brahmaputra River system. Earth Planet. Sci. Lett. 285 (1–2), 150–162.
Cottle, J.M., Waters, D.J., Riley, D., Beyssac, O., Jessup, M.J., 2011. Metamorphic history of the south Tibetan Detachment System, Mt. Everst Region, Revealed by RSCM Thermometry and phase equilibria modeling. J. Metamorph. Geol. 29 (5), 561–582.
Cottle, J.M., Searle, M.P., Jessup, M.J., Crowley, J.L., Law, R.D., 2015. Rongbuk re-visited: Geochronology of leucogranites in the footwall of the South Tibetan Detachment System, Everest Region, Southern Tibet. Lithos 227, 94–106.
DeCelles, P.G., Gehrels, G.E., Quade, J., Lareau, B., Spurlin, M., 2000. Tectonic implications of U-Pb zircon ages of the Himalayan Orogenic Belt in Nepal. Science 288 (5465), 497–499.
DeCelles, P.G., Gehrels, G.E., Najman, Y., Martin, A.J., Carter, A., Garzanti, E., 2004. Detrital geochronology and geochemistry of cretaceous early Miocene strata of Nepal: implications for timing and diachroneity of initial Himalayan orogenesis. Earth Planet. Sci. Lett. 227 (3), 313–330.
DeCelles, P.G., Kapp, P., Gehrels, G.E., Ding, L., 2014. Paleocene-Eocene foreland basin evolution in the Himalaya of southern Tibet and Nepal: implications for the age of initial India-Asia collision. Tectonics 33 (5), 824–849.
Dickinson, W.R., 1985. Interpreting provenance relations from detrital modes of sandstones. In: Zuffa, G.G. (Ed.), Provenance of Arenites: Proceeding of the NATO Advanced Study Institute on Reading Provenance from Arenites. Cosenza, Italy, pp. 333–361.
Dickinson, W.R., 1988. Provenance and Sediment Dispersal in Relation to Paleotectonics and Paleogeography of Sedimentary Basins, in New Perspectives in Basin Analysis. Spring, NewYork, pp. 3–25.
Dickinson, W.R., 2008. Impact of differential zircon fertility of granitoid basement rocks in North America on age populations of detrital zircons and implications for granite petrogenesis. Earth Planet. Sci. Lett. 275 (1–2), 80–92.
Dickinson, W.R., Gehrels, G.E., 2009. Use of U-Pb ages of detrital zircons to infer maximum depositional ages of strata: a test against a Colorado Plateau Mesozoic database. Earth Planet. Sci. Lett. 288 (1–2), 115–125.
Ding, L., Kapp, P., Zhong, D.L., Deng, W.M., 2003. Cenozoic Volcanism in Tibet: evidence for a transition from Oceanic to Continental Subduction. J. Petrol. 44 (10), 1833–1865.
Dong, X., Zhang, Z.M., Liu, F., Wang, W., Yu, F., Shen, K., 2011. Zircon U–Pb geochronology of the Nyainqentanglha Group from the Lhasa terrane: new constraints on the Triassic orogeny of the South Tibet. J. Asian Earth Sci. 42 (4), 732–739.
Fedo, C.M., Sircombe, K.N., Rainbird, R.H., 2003. Detrital zircon analysis of the sedimentary record. Rev. Miner. Geochem. 53 (1), 277–303.
Fu, Y., Sun, X.M., Zhou, H.Y., Lin, H., Yang, T.J., 2016. In-situ LA–ICP–MS U–Pb geochronology and trace elements analysis of polygenetic titanite from the giant Beiya gold–polymetallic deposit in Yunnan Province, Southwest China. Ore Geol. Rev. 77, 43–56.
Galehouse, J.S., 1974. Point counting. In: Carver, R.E. (Ed.), Procedures in Sedimentary Petrology. Wiley, New York, pp. 385–407.
Gansser, A., 1964. Geology of the Himalayas. Interscience, New York.
Gao, X.Y., Zheng, Y.F., Chen, Y.X., Guo, J.l., 2012. Geochemical and U–Pb age constraints on the occurrence of polygenetic titanites in UHP metagranite in the Dabie orogen. Lithos 136-139, 93–108.
Garzanti, E., 2016. From static to dynamic provenance analysis—sedimentary petrology upgraded. Sediment. Geol. 336, 3–13.
Garzanti, E., 2019. Petrographic classification of sand and sandstone. Earth Sci. Rev. 192, 545–563.
Garzanti, E., Andò, S., 2019. Heavy Minerals for Junior Woodchucks. Minerals 9, 148.
Garzanti, E., Casnedi, R., Jadoul, F., 1986. Sedimentary evidence of a Cambro-Ordovician orogenic event in the northwestern Himalaya. Sediment. Geol. 48 (3–4), 237–265.
Garzanti, E., Baud, A., Mascle, G., 1987. Sedimentary record of the northward flight of India and its collision with Eurasia (Ladakh Himalaya, India). Geodin. Acta 1 (4–5), 297–312.
Garzanti, E., Le Fort, P., Sciunnach, D., 1999. First report of lower Permian basalts in South Tibet: tholeiitic magmatism during break-up and incipient opening of Neotethys. J. Asian Earth Sci. 17 (4), 533–546.
Garzanti, E., Doglioni, C., Vezzoli, G., Andò, S., 2007. Orogenic Belts and Orogenic Sediment Provenance. J. Geol. 115 (3), 315–334.
Garzanti, E., Vermeesch, P., Andò, S., Vezzoli, G., Valagussa, M., Allen, K., Kadi, K.A., Al-Juboury, A.I.A., 2013. Provenance and recycling of Arabian desert sand. Earth-Sci. Rev. 120, 1–19.
Garzanti, E., Vermeesch, P., Rittner, M., Simmons, M., 2018. The zircon story of the Nile: time-structure maps of source rocks and discontinuous propagation of detrital signals. Basin Res. 30 (6), 1098–1117.
Garzanti, E., Limonta, M., Vezzoli, G., An, W., Wang, J.G., Hu, X.M., 2019. Petrology and multimineral fingerprinting of modern sand generated from a dissected magmatic arc (Lhasa River, Tibet). In: Ingersoll, R.V., Lawton, T.F., Graham, S.A. (Eds.), Tectonics, Sedimentary Basins, and Provenance: A Celebration of William R. Dickinson's Career: Geological Society of America Special Paper 540pp. 197–221.
Gehrels, G.E., Dickinson, W.R., Ross, G.M., Stewart, J.H., Howell, D.G., 1995. Detrital zircon reference for Cambrian to Triassic miogeoclinal strata of western North America. Geology 23 (9), 831–834.
Gehrels, G.E., Kapp, P., DeCelles, P., Pullen, A., Blakey, R., Weislogel, A., Ding, L., Guynn, J., Martin, A., Mcquarrie, N., 2011. Detrital zircon geochronology of pre-Tertiary strata in the Tibetan-Himalayan orogen. Tectonics 30 (5), TC5016.
Goscombe, B., Gray, D., Foster, D.A., 2018. Metamorphic response to collision in the Central Himalayan Orogen. Gondwana Res. 57, 191–265.
Griffin, W.L., Powell, W.J., Pearson, N.J., O'Reilly, S.Y., 2008. GLITTER: data reduction software for laser ablation ICP-MS. Short Course Ser. 40, 308–311.
Grimes, C.B., John, B.E., Kelemen, P.B., Mazdab, F.K., Wooden, J.L., Cheadle, M.J., Hanghøj, K., Schwartz, J.J., 2007. Trace element chemistry of zircons from oceanic crust: a method for distinguishing detrital zircon provenance. Geology 35 (7), 643–646.
Hacker, B.R., Kelemen, P.B., Behn, M.D., 2011. Differentiation of the continental crust by relamination. Earth Planet. Sci. Lett. 307 (3), 501–516.
Harrison, T.M., Grove, M., Lovera, O.M., Catlos, E.J., 1998. A model for the origin of Himalayan anatexis and inverted metamorphism. J. Geophys. Res. Solid Earth 103 (B11), 27017–27032.
Hartmann, L.o.A., Santos, J.o.O.S., 2004. Predominance of high Th/U, magmatic zircon in Brazilian Shield sandstones. Geology 32 (1), 73–76.
Hawkesworth, C., Cawood, P., Kemp, T., Storey, C., Dhuime, B., 2009. A matter of preservation. Science 323 (5910), 49–50.
He, M.Y., Zheng, H.B., Bookhagen, B., Clift, P.D., 2014. Controls on erosion intensity in the Yangtze River basin tracked by U–Pb detrital zircon dating. Earth-Sci. Rev. 136, 121–140.
Hietpas, J., Samson, S., Moecher, D., Schmitt, A.K., 2010. Recovering tectonic events from the sedimentary record: Detrital monazite plays in high fidelity. Geology 38 (2), 167–170.
Hu, D.G., Wu, Z.H., Ye, P.S., Jiang, W., 2003. SHRIMP U-Pb ages of zircons from dioritic gneiss in the Nyainqentanglha Mountains, Tibet. Reg. Geol. China 22 (11 − 12), 936–940.
Hu, X.M., Jansa, L., Chen, L., Griffin, W.L., O'Reilly, S.Y., Wang, J.G., 2010. Provenance of lower cretaceous Wölong Volcaniclastics in the Tibetan Tethyan Himalaya: implications for the final breakup of Eastern Gondwana. Sediment. Geol. 223 (3), 193–205.
Hu, X.M., Garzanti, E., Moore, T., Raffi, I., 2015a. Direct stratigraphic dating of India-Asia collision onset at the Selandian (middle Paleocene, 59 ± 1 Ma). Geology 43 (10), 859–862.
Hu, X.M., Garzanti, E., An, W., Hu, X.F., 2015b. Provenance and drainage system of the early cretaceous volcanic detritus in the Himalaya as constrained by detrital zircon geochronology. J. Palaeogeogr. 4 (1), 85–98.
Hu, X.M., Garzanti, E., Wang, J.G., Huang, W.T., An, W., Webb, A., 2016. The timing of India-Asia collision onset – facts, theories, controversies. Earth-Sci. Rev. 160, 264–299.
Ingersoll, R.V., Bullard, T.F., Ford, R.L., Pickle, J.D., 1985. The effect of grain size on detrital modes; a test of the Gazzi-Dickinson point-counting method. J. Sediment. Res. 54 (4), 616–618.
Itano, K., Iizuka, T., Chang, Q., Kimura, J.I., Maruyama, S., 2016. U–Pb chronology and geochemistry of detrital monazites from major African rivers: constraints on the timing and nature of the Pan-African Orogeny. Precambrian Res. 282, 139–156.
Jackson, S., Pearson, J., Griffin, W., Belousova, E., 2004. The application of laser ablation-inductively coupled plasma-mass spectrometry to in situ U-Pb zircon geochronology. Chem. Geol. 211, 47–69.
Jadoul, F., Berra, F., Garzanti, E., 1998. The Tethys Himalayan passive margin from late Triassic to early cretaceous (South Tibet). J. Asian Earth Sci. 16 (2–3), 173–194.
Jarvis, A., Reuter, H.I., Nelson, A., E, G., 2008. Hole-Filled Seamless SRTM Data V4. International Centre for Tropical Agriculture (CIAT) available from. http://srtm.csi.cgiar.org.
Ji, W.Q., Wu, F.Y., Chung, S.L., Li, J.X., Liu, C.Z., 2009. Zircon U–Pb geochronology and Hf isotopic constraints on petrogenesis of the Gangdese batholith, southern Tibet. Chem. Geol. 262 (3), 229–245.
Ji, W.Q., Wu, F.Y., Chung, S.L., Wang, X.C., Liu, C.Z., Li, Q.L., Liu, Z.C., Liu, X.C., Wang, J.G., 2016. Eocene Neo-Tethyan slab breakoff constrained by 45 Ma oceanic island basalt-type magmatism in southern Tibet. Geology 44 (4), G37612.1.
Jonell, T.N., Carter, A., Böning, P., Pahnke, K., Clift, P.D., 2017. Climatic and glacial impact on erosion patterns and sediment provenance in the Himalayan rain shadow, Zanskar River, NW India. Geol. Soc. Am. Bull. 129 (7–8), 820–836.
Kapp, P., DeCelles, P.G., 2019. Mesozoic–Cenozoic geological evolution of the Himalayan-Tibetan orogen and working tectonic hypotheses. Am. J. Sci. 319 (3), 159–254.
Kapp, J.L.D.A., Harrison, T.M., Kapp, P., Grove, M., Lovera, O.M., Lin, D., 2005. Nyainqentanglha Shan: a window into the tectonic, thermal, and geochemical evolution of the Lhasa block, southern Tibet. J. Geophys. Res. Solid Earth 110 (B8).
Kennedy, A., Nasdala, L., 2002. Grenville skarn titanite: potential reference material for SIMS U-Th-Pb analysis. Can. Mineral 2010 (48), 1423–1443.
King, J., Harris, N., Argles, T., Parrish, R., Zhang, H.F., 2011. Contribution of crustal anatexis to the tectonic evolution of Indian crust beneath Southern Tibet. Geol. Soc.

Am. Bull. 123 (1), 218–239.
Kohn, M.J., 2014. Himalayan metamorphism and its tectonic implications. Annu. Rev. Earth Planet. Sci. 42 (1), 381–419.
Lang, K.A., Huntington, K.W., Montgomery, D.R., 2013. Erosion of the Tsangpo Gorge by megafloods, Eastern Himalaya. Geology 41 (9), 1003–1006.
Lee, J., Hacker, B.R., Dinklage, W.S., Wang, Y., Gans, P., Calvert, A., Wan, J.L., Chen, W., Blythe, A.E., Mcclelland, W., 2000. Evolution of the Kangmar Dome, southern Tibet: structural, petrologic, and thermochronologic constraints. Tectonics 19 (5), 872–895.
Lee, J., Hacker, B., Yu, W., 2004. Evolution of North Himalayan gneiss domes: structural and metamorphic studies in Mabja Dome, southern Tibet. J. Struct. Geol. 26 (12), 2297–2316.
Lee, J., McCleland, W., Wang, Y., Blythe, A., McWilliams, M., 2006. Oligocene–Miocene middle crustal flow in southern Tibet: geochronology of Mabja Dome. Geol. Soc. Lond., Spec. Publ. 268, 445–469.
Leier, A.L., Kapp, P., Gehrels, G.E., DeCelles, P.G., 2010. Detrital zircon geochronology of Carboniferous-cretaceous strata in the Lhasa terrane, Southern Tibet. Basin Res. 19 (3), 361–378.
Leloup, P.H., Mahéo, G., Arnaud, N., Kali, E., Boutonnet, E., Liu, D.Y., Liu, X.H., Li, H.B., 2010. The South Tibet detachment shear zone in the Dinggye area: time constraints on extrusion models of the Himalayas. Earth Planet. Sci. Lett. 292, 1): 1–16.
Li, W.C., Zhang, Z.M., Hua, X., Gou, Z.B., Ding, H.X., 2015. Metamorphism and anatexis of the Himalayan orogen: petrology and geochronology of HP pelitic granulites from the Yadong area, Southern Tibet. Acta Petrol. Sin. 31 (05), 1219–1234.
Liu, D., Zhao, Z.D., Zhu, D.C., Wang, Q., Sui, Q.L., Liu, Y.S., 2011. The petrogenesis of postcollisional potassic-ultrapotassic rocks in Xungba basin, western Lhasa terrane: Constraints from zircon U-Pb geochronology and geochemistry. Acta Petrol. Sin. 27 (7), 2045–2059.
Liu, Z.C., Wu, F.Y., Yang, Y.H., Yang, J.H., Wilde, S.A., 2012. Neodymium isotopic compositions of the standard monazites used in U Th Pb geochronology. Chem. Geol. 334 (1), 221–239.
Liu, X.C., Wu, F.Y., Yu, L.J., Liu, Z.C., Ji, W.Q., Wang, J.G., 2016. Emplacement age of leucogranite in the Kampa Dome, southern Tibet. Tectonophysics 667, 163–175.
Liu, X.C., Wu, Y.B., Fisher, C.M., Hanchar, J.M., Beranek, L., Gao, S., Wang, H., 2017. Tracing crustal evolution by U-Th-Pb, Sm-Nd, and Lu-Hf isotopes in detrital monazite and zircon from modern rivers. Geology 45 (2), 103–106.
Luvizotto, G.L., Zack, T., Meyer, H.P., Ludwig, T., Triebold, S., Kronz, A., Münker, C., Stockli, D.F., Prowatke, S., Klemme, S., 2009. Rutile crystals as potential trace element and isotope mineral standards for microanalysis. Chem. Geol. 261 (3), 346–369.
Malusà, M.G., Garzanti, E., 2019. The sedimentology of detrital thermochronology. In: Fission-Track Thermochronology and its Application to Geology. Springer, pp. 123–143.
Malusà, M.G., Resentini, A., Garzanti, E., 2016. Hydraulic sorting and mineral fertility bias in detrital geochronology. Gondwana Res. 31, 1–19.
Malusà, M.G., Wang, J., Garzanti, E., Liu, Z.C., Villa, I.M., Wittmann, H.J.L., 2017. Trace-element and Nd-isotope systematics in detrital apatite of the Po river catchment: implications for provenance discrimination and the lag-time approach to detrital thermochronology. Lithos 290, 48–59.
Mange, M.A., Morton, A.C., 2007. Chapter 13 Geochemistry of heavy minerals. Dev. Sedimentol. 58, 345–391.
Mazdab, F.K., Wooden, J.L., Barth, A.P., 2007. Trace element variability in titanite from diverse geologic environments. Geol. Soc. Am. Abstr. Programs 39, 406.
Meinhold, G., 2010. Rutile and its applications in earth sciences. Earth-Sci. Rev. 102, 1–28.
Meinhold, G., Anders, B., Kostopoulos, D., Reischmann, T., 2008. Rutile chemistry and thermometry as provenance indicator: an example from Chios Island, Greece. Sediment. Geol. 203 (1), 98–111.
Miller, C., Schuster, R., Klötzli, U., Frank, W., Purtscheller, F., 1999. Post-collisional potassic and ultrapotassic magmatism in SW Tibet: geochemical and Sr–Nd–Pb–O isotopic constraints for mantle source characteristics and petrogenesis. J. Petrol. 40 (9), 699–715.
Moecher, D.P., Samson, S.D., 2006. Differential zircon fertility of source terranes and natural bias in the detrital zircon record: Implications for sedimentary provenance analysis. Earth Planet. Sci. Lett. 247 (3), 252–266.
Molinaroli, E., Basu, A., 1993. Toward quantitative provenance analysis: a brief review and case study. Spec. Pap. Geol. Soc. Am. 284, 323–333.
Morton, A.C., 1991. Geochemical studies of detrital heavy minerals and their application to provenance research. Geol. Soc. Lond., Spec. Publ. 57 (1), 31–45.
Morton, A.C., Hallsworth, C., 2007. Stability of detrital heavy minerals during burial diagenesis. Heavy Miner. Use 58, 215–245.
Mottram, C.M., Cottle, J.M., Kylander-Clark, A.R.C., 2018. Campaign-style U-Pb titanite petrochronology: along-strike variations in timing of metamorphism in the Himalayan metamorphic core. Geosci. Front. 10 (3), 827–847.
O'Sullivan, G.J., Chew, D.M., Samson, S.D., 2017. Sediment provenance in contractional orogens: the detrital zircon record from modern rivers in the Andean fold-thrust belt and foreland basin of western Argentina. Earth Planet. Sci. Lett. 479, 83–97.
Pan, G.T., Yao, D.S., Wang, L.Q., 2004. Geological Map of Qinghai-Xizang (Tibet) Plateau and Adjacent Areas (1:1,500,000). Chengdu Cartographic Publishing House, Chengdu.
Paton, C., Woodhead, J.D., Hellstrom, J.C., Hergt, J.M., Greig, A., Maas, R., 2010. Improved laser ablation U-Pb zircon geochronology through robust downhole fractionation correction. Geochem. Geophys. Geosyst. 11 (3), 1–36.
Peterman, E.M., 2005. Monazite standard assessment by LA-ICP-MS. Geol. Soc. Am. Abstr. Programs 37, 448.
Potter, P.E., 1994. Modern sands of South America: composition, provenance and global significance. Geol. Rundsch. 83 (83), 212–232.
Qiu, K.F., Yang, L.Q., 2011. Genetic feature of monazie and its U-Th-Pb dating: critical considerations on the tectonics evolution of Sanjiang Tethys. Acta Petrol. Sin. 27 (9), 2721–2732.
Rahl, J.M., Ehlers, T.A., van der Pluijm, B.A., 2007. Quantifying transient erosion of orogens with detrital thermochronology from syntectonic basin deposits. Earth Planet. Sci. Lett. 256 (1), 147–161.
Ratschbacher, L., Frisch, W., Liu, G.H., Chen, C.S., 1994. Distributed deformation in Southern and Western Tibet during and after the India-Asia collision. J. Geophys. Res. Solid Earth 99 (B10), 19917–19945.
Rubatto, D., 2002. Zircon trace element geochemistry: partitioning with garnet and the link between U–Pb ages and metamorphism. Chem. Geol. 184 (1), 123–138.
Rudnick, R.L., Gao, S., 2003. The composition of the continental crust. Treat. Geochem. 3, 1–64.
Saylor, J.E., Knowles, J.N., Horton, B.K., Nie, J., Mora, A., 2013. Mixing of source populations recorded in detrital zircon U-Pb age spectra of modern river sands. J. Geol. 121 (1), 17–33.
Schärer, U., Xu, R.H., Allègre, C.J., 1986. U(Th)Pb systematics and ages of Himalayan leucogranites, South Tibet. Earth Planet. Sci. Lett. 77 (1), 35–48.
Sciunnach, D., Garzanti, E., 2012. Subsidence history of the Tethys Himalaya. Earth-Sci. Rev. 111 (1–2), 179–198.
Shi, G.H., Li, X.H., Li, Q.L., Chen, Z.Y., Deng, J., Liu, Y.X., Kang, Z.J., Pang, E.C., Xu, Y.J., Jia, X.M., 2012. Ion microprobe U-Pb age and Zr-in-Rutile thermometry of rutiles from the daixian rutile deposit in the Hengshan Mountains, Shanxi Province, China. Econ. Geol. 107 (3), 525–535.
Spencer, C.J., Kirkland, C.L., Roberts, N.M.W., 2018. Implications of erosion and bedrock composition on zircon fertility: examples from South America and Western Australia. Terra Nova 30 (4), 289–295.
Stock, G.M., Ehlers, T.A., Farley, K.A., 2006. Where does sediment come from? Quantifying catchment erosion with detrital apatite (U-Th)/He thermochronometry. Geology 34 (9), 725–728.
Streule, M.J., Searle, M.P., Waters, D.J., Horstwood, M.S.J.T., 2010. Metamorphism, melting, and channel flow in the Greater Himalayan Sequence and Makalu leucogranite: Constraints from thermobarometry, metamorphic modeling, and U-Pb geochronology. Tectonics 29, TC50011.
Sun, S.S., McDonough, W.F., 1989. Chemical and isotopic systematics of oceanic basalts: implications for mantle composition and processes. Geol. Soc. Lond., Spec. Publ. 42 (1), 313–345.
Sun, J.F., Yang, J.H., Wu, F.Y., Xie, L.W., Yang, Y.H., Liu, Z.C., Li, X.H., 2012. In situ U-Pb dating of titanite by LA-ICPMS. Sci. Bull. 57 (20), 2506–2516.
Suzuki, K., Adachi, M., 1991. Precambrian provenance and Silurian metamorphism of the Tsubonosawa paragneiss in the South Kitakami terrane, Northeast Japan, revealed by the chemical Th-U-total Pb isochron ages of monazite, zircon and xenotime. Geochem. J. 25 (5), 357–376.
Thomsen, T.B., Knudsen, C., Hinchey, A.M., 2015. Investigations of detrital zircon, rutile and titanite from present-day Labrador drainage basins: fingerprinting the Grenvillean front. Geol. Surv. Denmark Greenl. Bull. 33, 77–80.
Triebold, S., Eynatten, H.V., Luvizotto, G.L., Zack, T., 2007. Deducing source rock lithology from detrital rutile geochemistry: An example from the Erzgebirge, Germany. Chem. Geol. 244 (3), 421–436.
Triebold, S., Eynatten, H.V., Zack, T., 2012. A recipe for the use of rutile in sedimentary provenance analysis. Sediment. Geol. 282, 268–275.
Turner, S., Hawkesworth, C., Liu, J., Rogers, N., Kelley, S., van Calsteren, P., 1993. Timing of Tibetan uplift constrained by analysis of volcanic rocks. Nature 364 (6432), 50–54.
Vermeesch, P., 2012. On the visualisation of detrital age distributions. Chem. Geol. 312–313 (3), 190–194.
Vezzoli, G., Limonta, M., Garzanti, E., Yang, S., 2016a. Quantitative provenance analysis of sediments in the Changjiang (Yangtze) river (China). In: Geostatistical and Geospatial Approaches for the Characterization of Natural Resources in the Environment. Springer International Publishing, Cham, pp. 293–300.
Vezzoli, G., Garzanti, E., Limonta, M., Andò, S., Yang, S., 2016b. Erosion patterns in the Changjiang (Yangtze River) catchment revealed by bulk-sample versus single-mineral provenance budgets. Geomorphology 261, 177–192.
Wang, J.G., Hu, X.M., 2008. Applications of geochemistry and geochronology accessory minerals in sandstones to provenance analysis. Geol. Rev. 54 (5), 670–678.
Wang, X.X., Zhang, J., Yan, S.Y., Liu, J., 2015. Structrual characteristics and active time of the Kangmar detachment, Southern Tibet. Geotecton. Metallog. 39 (2), 250–259.
Watson, E.B., 1979. Zircon saturation in felsic liquids: experimental results and applications to trace element geochemistry. Contrib. Miner. Petrol. 70 (4), 407–419.
Weltje, G.J., 2012. Quantitative models of sediment generation and provenance: State of the art and future developments. Sediment. Geol. 280, 4–20.
Weltje, G.J., von Eynatten, H., 2004. Quantitative provenance analysis of sediments: review and outlook. Sediment. Geol. 171 (1), 1–11.
Wen, D.R., Liu, D.Y., Chung, S.L., Chu, M.F., Jianqing, J.I., Zhang, Q.I., Song, B., 2008. Zircon SHRIMP U-Pb ages of the Gangdese Batholith and implications for Neotethyan subduction in southern Tibet. Chem. Geol. 252 (3), 191–201.
Williams, M.L., Jercinovic, M.J., Hetherington, C., 2007. Microprobe monazite geochronology: understanding geologic processes by integrating composition and chronology. Annu. Rev. Earth Planet. Sci. 35, 137–175.
Woodhead, J.D., Hellstrom, J., Hergt, J.M., Greig, A., Maas, R., 2007. Isotopic and elemental imaging of geological materials by laser ablation inductively coupled plasma-mass spectrometry. Geostand. Geoanal. Res. 31 (4), 331–343.
Wu, C.D., D, N.K., Greg, W., Yue, Y.J., Li, J.X., A, E.M., 1998. Yadong cross structure and South Tibetan Detachment in the east central Himalaya (89°-90°E). Tectonics 17 (1), 28–45.
Wu, F.Y., Ji, W.Q., Wang, J.G., Liu, C.Z., Chung, S.L., Clift, P.D., 2014. Zircon U–Pb and Hf isotopic constraints on the onset time of India-Asia collision. Am. J. Sci. 314 (2),

548–579.
Wu, F.Y., Liu, Z.C., Liu, X.C., Ji, W.Q., 2015. Himalaya Leucogranite: petrogenesis and implication to orogenesis and plateu uplift. Acta Petrol. Sin. 31 (1), 1–36.
Xie, F.W., Tang, J.X., Lang, X.H., Ma, D., 2018. The different sources and petrogenesis of Jurassic intrusive rocks in the southern Lhasa subterrane, Tibet: evidence from the trace element compositions of zircon, apatite, and titanite. Lithos 314–315, 447–462.
Xu, R.H., Schärer, U., Allègre, C.J., 1985. Magmatism and Metamorphism in the Lhasa Block (Tibet): a Geochronological Study. J. Geol. 93 (1), 41–57.
Yin, A., Dubey, C., Kelty, T., Gehrels, G.E., Chou, C., Grove, M., Lovera, O., 2006. Structural evolution of the Arunachal Himalaya and implications for asymmetric development of the Himalayan orogen. Curr. Sci. 90, 195–206.
Zack, T., 2017. Petrology and geochronology of rutile. Rev. Mineral. Geochem. 83, 443–467.
Zack, T., Eynatten, H.V., Kronz, A., 2004. Rutile geochemistry and its potential use in quantitative provenance studies. Sediment. Geol. 171 (1), 37–58.
Zeng, L.S., Gao, L.E., Xie, K., Jing, L.Z., 2011. Mid-Eocene high Sr/Y granites in the Northern Himalayan Gneiss Domes: melting thickened lower continental crust. Earth Planet. Sci. Lett. 303 (3–4), 251–266.
Zhang, H.F., Harris, N., Parrish, R., Zhang, L., Zhao, Z.D., 2005. Geochemistry of North Himalayan Leucogranites: regional comparison, petrogenesis and tectonic implications. Earth Sci. J. China Univ. Geosci. 30 (3), 275–288.
Zhang, J.Y., Yin, A., Wu, F.Y., Ding, L., M, G., 2012. Coupled U-Pb dating and Hf isotopic analysis of detrital zircons from modern sand of the Yalu River System (Yarlung Tsangpo) in Southern Tibet: implications for Himalayan Provenance analysis and drainage reconstruction. Geol. Soc. Am. Bull. 124 (9–10), 1449–1473.
Zhang, Z.M., Dong, X., Santosh, M., Zhao, G.C., 2014. Metamorphism and tectonic evolution of the Lhasa terrane, Central Tibet. Gondwana Res. 25 (1), 170–189.
Zhang, Z.M., Xiang, H., Dong, X., Li, W.C., Ding, H., Gou, Z.B., Tian, Z.L., 2015. Oligocene HP metamorphism and anatexis of the higher Himalayan Crystalline Sequence in Yadong region, east-central Himalaya. Gondwana Res. 41, 173–187.
Zhang, H.Z., Lu, H.Y., Xu, X.S., Liu, X.M., Yang, T., Stevens, T., Bird, A., Xu, Z.W., Zhang, T., Lei, F., Feng, H., 2016. Quantitative estimation of the contribution of dust sources to Chinese loess using detrital zircon U-Pb age patterns. J. Geophys. Res. 121 (11), 2085–2099.
Zhao, Z.D., Mo, X.X., Dilek, Y., Niu, Y.L., Depaolo, D.J., Robinson, P.T., Zhu, D.C., Sun, C.G., Dong, G.C., Su, Z., 2009. Geochemical and Sr-Nd-Pb-O isotopic compositions of the post-collisional ultrapotassic magmatism in SW Tibet; petrogenesis and implications for India intra-continental subduction beneath southern Tibet. Lithos 113 (1), 190–212.
Zhu, D.C., Pan, G.T., Mo, X.X., Wang, L.Q., Liao, Z.L., Jiang, X.S., Geng, Q.R., 2005. SHRIMP U-Pb zircon dating for the dacite of the Sangxiu Formation in the central segment of Tethyan Himalaya and its implications. Chin. Sci. Bull. 50 (6), 69–74.
Zhu, D.C., Pan, G.T., Mo, X.X., Liao, Z.L., Jiang, X.S., Wang, L.Q., Zhao, Z.D., 2007. Petrogenesis of volcanic rocks in the Sangxiu Formation, central segment of Tethyan Himalaya: a probable example of plume–lithosphere interaction. J. Asian Earth Sci. 29 (2), 320–335.
Zhu, D.C., Chung, S.L., Mo, X.X., Zhao, Z.D., Niu, Y.L., Song, B., Yang, Y.H., 2009. The 132 Ma Comei-Bunbury large igneous province: Remnants identified in present-day southeastern Tibet and southwestern Australia. Geology 37 (7), 583–586.
Zhu, D.C., Zhao, Z.D., Niu, Y., Mo, X.X., Chung, S.L., Hou, Z.Q., Wang, L.Q., Wu, F.Y., 2011. The Lhasa Terrane: Record of a microcontinent and its histories of drift and growth. Earth Planet. Sci. Lett. 301 (1–2), 241–255.
Zhu, D.C., Zhao, Z.D., Niu, Y.L., Dilek, Y., Hou, Z.Q., Mo, X.X., 2013. The origin and pre-Cenozoic evolution of the Tibetan Plateau. Gondwana Res. 23 (4), 1429–1454.
Zhu, D.C., Wang, Q., Zhao, Z.D., Chung, S.L., Cawood, P.A., Niu, Y., Liu, S.A., Wu, F.Y., Mo, X.X., 2015. Magmatic record of India-Asia collision. Sci. Rep. 5, 14289.
Zhu, D.C., Wang, Q., Chung, S.L., Cawood, P.A., Zhao, Z.D., 2019. Gangdese magmatism in southern Tibet and India–Asia convergence since 120 Ma. Geol. Soc. Lond., Spec. Publ. 483, SP483.14.